

APPENDIX F

THE DEVELOPMENT OF A J-ESTIMATION SCHEME FOR CIRCUMFERENTIAL AND AXIAL THROUGH-WALL CRACKED ELBOWS

F.1 INTRODUCTION

Leak before break (LBB) considerations for pipe fittings such as tee joints and elbows have not been investigated in detail to date. Reference F.1 presented the development of a surface crack estimation scheme for elbows. These solutions were then used to investigate the possibility of using simple influence functions, based on ASME Section III stress indices, along with existing straight pipe solutions, to predict the fracture response of a surface-cracked elbow. The use of this small database of influence functions, combined with existing straight pipe J-estimation methods showed promise in predicting the fracture response of the surface-cracked elbows.

However, in order to perform LBB sensitivity studies on fittings, such as elbows, TWC solutions must be available. With the TWC elbow solutions available, one can investigate the feasibility of using influence functions and straight pipe TWC solutions to predict the LBB behavior of fittings. The main purpose of this effort is to provide a new J-estimation scheme for TWC elbows. Both circumferential and axial cracks are considered. In addition, crack-opening displacements can be estimated so that LBB considerations can be assessed.

F.2 BACKGROUND ON PIPING J-ESTIMATION SCHEMES

The nuclear industry has traditionally taken the lead in the development of J-estimation schemes to allow engineers to make estimates of the fracture behavior of nuclear piping components. These J-estimation schemes have permitted engineers to make simple fracture assessments of planar component geometries (Ref. F.2), through-wall-cracked (TWC) pipes (Ref. F.3), as well as surface-cracked (SC) pipe (Ref. F.4). This early work sometimes had inaccuracies implicit within the solutions, in part due to the fact that the finite element methods used at that time were not quite fully developed, nor as robust as today's numerical tools.

Corrections and improvements to pipe fracture J-estimation schemes were made subsequent to

this original work. References F.5 and F.6 represent the development of alternative J-estimation schemes for TWC pipe which are not based on the compilation of a series of numerical solutions; rather these solutions were developed from making certain geometric assumptions. References F.7 and F.8 are similar non-finite element based J-estimation schemes for surface cracked pipe. References F.9 and F.10 represent the improvements and corrections to the original numerical solutions using improved numerical finite element techniques (compared with the original solutions) and permitted pipes with "small" cracks to be more accurately modeled. In addition, some of these methods were specifically developed to account for cracks in welds (Refs. F.8 and F.11). References F.8 to F.12, and many references cited therein, summarize many of these methods, both numerical and engineering based, and compare predictions to full-scale experimental test data.

The J-estimation schemes discussed above were appropriate for cracked pipe. Fracture estimates for more complicated geometries, such as pipe fittings, had to be performed on a case-by-case basis using finite element analysis. These analyses are time consuming, often requiring significant resources, and the results are only appropriate for the specific geometry and material considered. As such, the development of more general J-estimation schemes for pipe fittings, such as elbows and Tee joints, has begun. A surface crack estimation scheme for axial and circumferential cracked elbows was developed in Reference F.1.

The purpose of this effort is to develop a J-estimation scheme for axial and circumferential through-wall cracks in elbows. Solutions are compiled for the pure pressure, combined pressure and bending, and pure bending cases. However, before presenting these solutions, it is first instructive to discuss some unique features associated with fracture of elbows, which are not necessarily intuitive based on experience with straight pipe. Many of these anomalies are associated with the way that elbows ovalize.

F.3 GENERAL OVERVIEW OF DEFORMATION AND FRACTURE RESPONSE OF ELBOWS

F.3.1 Geometry

The geometry of the cracked elbows considered here is illustrated in Figure F.1. We are interested in estimating J and crack opening displacement (COD) for both circumferential and axial 'flank' cracks. The ratio of $R_{el}/R_m = 3$ here represents a long radius elbow. The loading cases considered are pure pressure, pure bending, and combined pressure and bending. The pressure loading turns out to be very important consideration for elbows. Note that the outer length of the elbow [i.e. $(R_{el} + R_m/2) * \psi$] is greater than the inner length of the elbow [i.e. $(R_{el} - R_m/2) * \psi$]. From the free body diagram alone, this means that the integrated pressure along the outer length of the elbow is greater than that along the inside of the elbow, i.e., there is a net outward force that must be equilibrated by the end cap pressure T (see Figure F.1). This means that, due to pressure alone, the elbow wants to straighten out. Therefore, for the cases of pressure and combined pressure and bending, both the pressure and end cap tension must be applied. This is not the case for a straight pipe, where the pressure can be neglected when developing J-estimation schemes for circumferential cracks. It turns out that the effect of pressure also has an important effect on the ovalization of the elbow, which in turn, affects the J- and COD- solutions.

F.3.2 Solution Procedure

Figure F.2 shows a typical finite element mesh that was used for the analyses. Figure F.2(a) shows an example of a 90-degree circumferential crack in an elbow. A quarter model, with symmetry about the plane of the crack and a symmetry plane about the half crack length, θ , was used to simplify the analyses. As seen in Figure F.2, a long length of straight pipe, equal to $L = 9 D$ (with D the diameter), was included in the model. At the end of the length of pipe, a series of very stiff beams were attached to the pipe, which met at a point node at the center of the pipe. The bending moment, M,

was applied at this node. The length, 9D, was determined by performing a series of mesh sensitivity studies. This technique simplified the analysis procedure, the reduction of data, and assured that the elbow solutions were not distorted by end effects. Figure F.2(b) shows a typical mesh for a 15-degree axial crack. For the axial cracks, half symmetry models were used. For both circumferential and axial cracks, pressure along the entire inside pipe and elbow surfaces were included along with end cap pressure at the end of the long length of straight pipe.

The ABAQUS commercial finite element package was used for all analyses. The 20-node isoparametric brick element was used for all solutions. A deformation theory plasticity model was used, although, as will be seen later, flow theory was used for some of validation studies. Because the ABAQUS deformation solution procedure includes the elastic strains, each solution was monitored and considered complete (i.e., fully plastic) when the plastic strain at each integration point became greater than ten times the elastic strain. As an independent check on the adequacy of the fully plastic solution, the h-functions (see next section), were plotted as a function of load at each load step in the analysis. Typically, h reached a constant, converged value long before the analysis was automatically completed using the criteria discussed above. The compilations of h-functions were performed using one element through the thickness, as illustrated in Figure F.3. However, as seen in Figure F.3(b) several solutions were performed using a mesh with four elements through the thickness. The average J-integral, and COD, solutions for the four elements through the thickness mesh compared well with the results for the one element mesh. It is noted that there is a variation of J through the thickness, especially for the axial flank cracks, but the use of one, average value for J, is adequate for engineering estimation purposes. An extensive mesh sensitivity study was performed to ensure adequate solution convergence. The procedure was also validated by comparing results for known straight pipe solutions. Because of the use of parabolic elements, the values of J for the

one element through the thickness meshes (Figure F.3(a)) were calculated using:

$$J_{AVG} = J_I + 4J_M + J_O \quad (F.1)$$

where J_I is the value of J at the inner surface node at the crack, J_M is J at the mid side node, and J_O is J at the outside node.

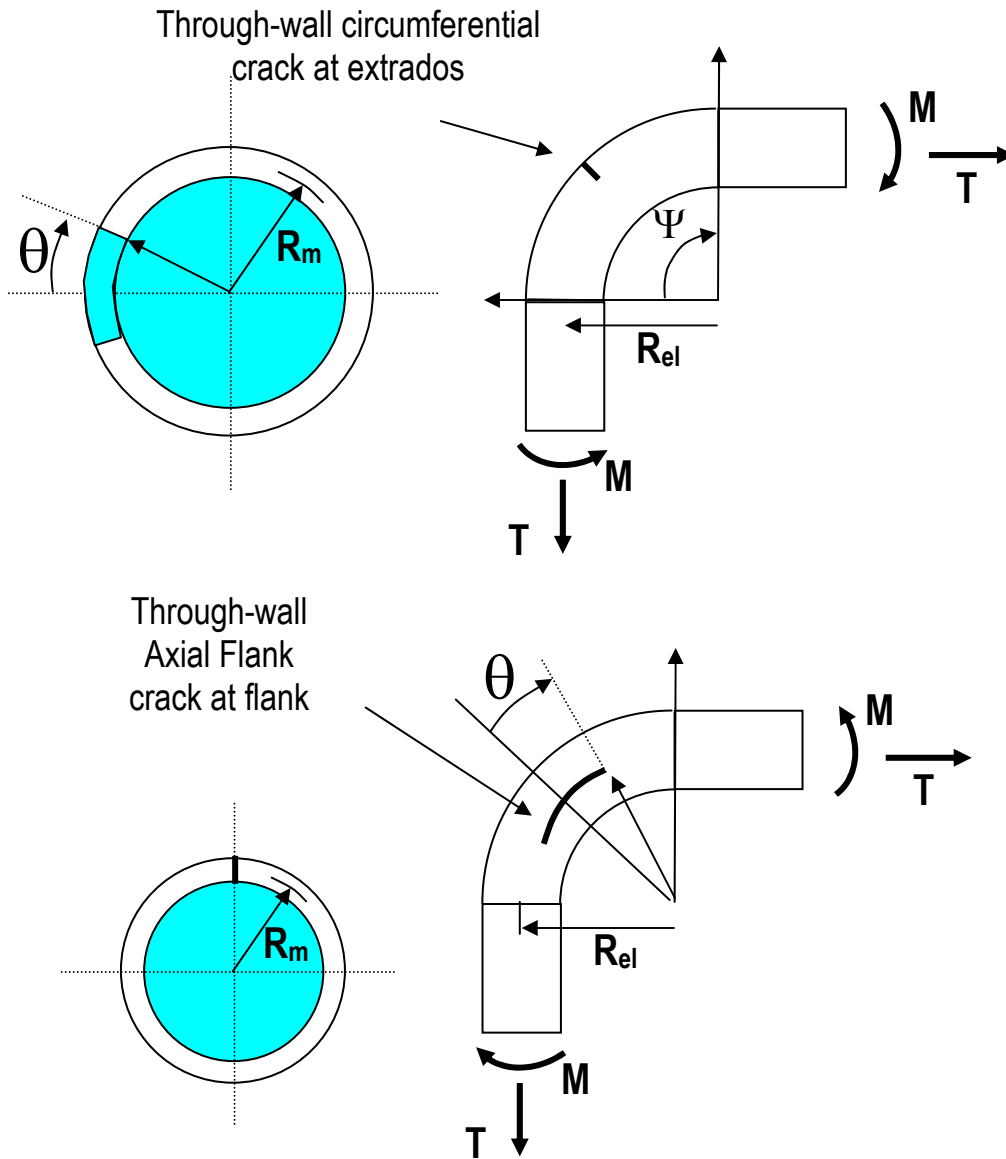
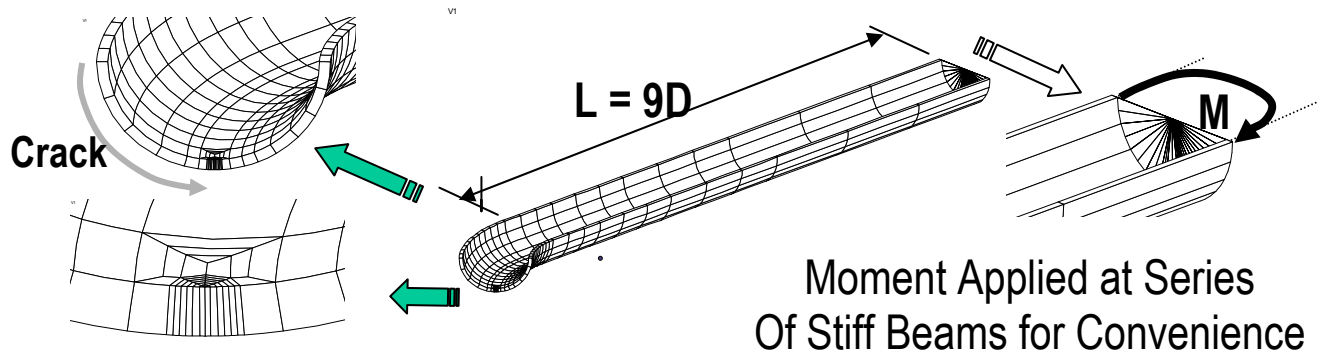
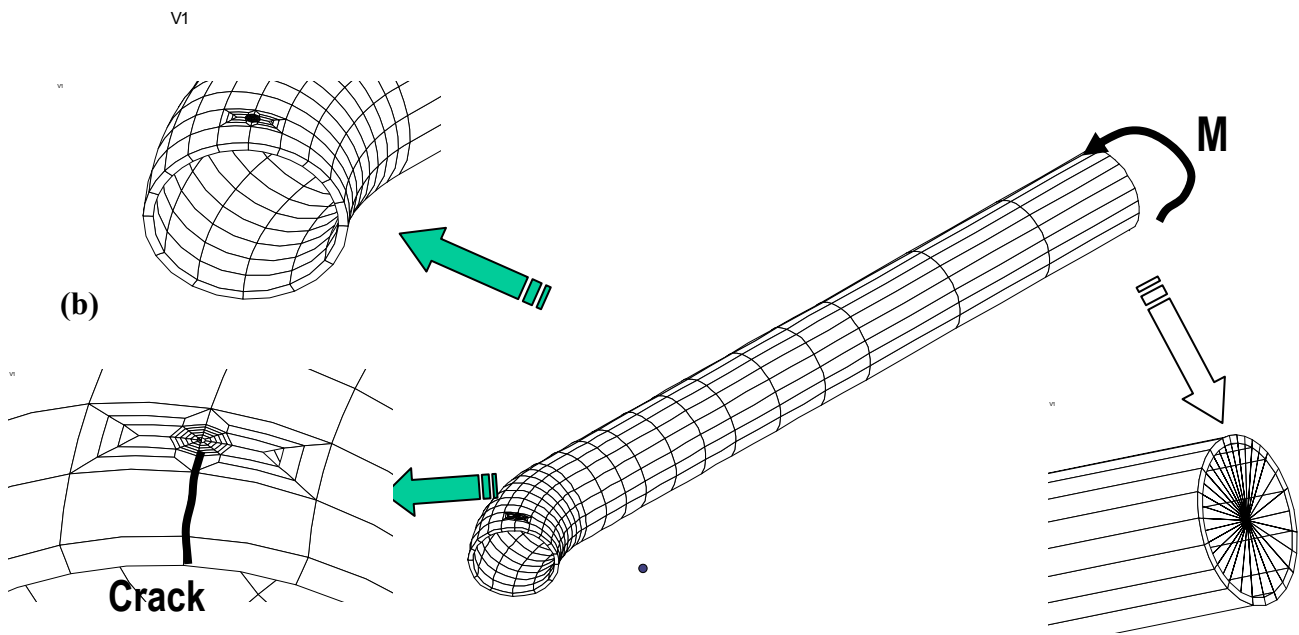


Figure F.1 Crack geometries considered for elbows



(a)



(b)

Figure F.2 Typical finite element mesh and model geometry for (a) a 90-degree circumferential crack and (b) a 15-degree axial flank crack

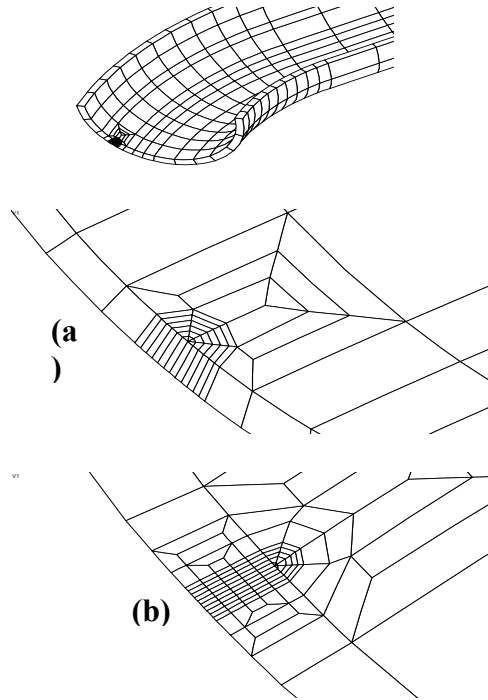


Figure F.3 Typical mesh (circumferential crack, 45-degree crack) (a) one element through thickness and (b) four elements through thickness

F.4 OVALIZATION EFFECTS ON ELBOW FRACTURE

F.4.1 Circumferential Cracks

The ovalizations induced in elbows that are subjected to bending loads turns out to have an important effect on the predicted J-integral, crack opening displacements, and fracture response. Consider the simple example of Figure F.4. In the upper plot (Figure F.4(a)), an illustration of a circumferentially cracked elbow subjected to a closing moment is shown. Intuitively, an elbow closing moment would be expected to open the crack, similar to what occurs in a straight length of pipe subjected to a crack opening moment. The illustration to the right in Figure F.4(a) shows a deformed plot caused by the applied moment. The shaded areas represent contour plots of the crack opening stress and the numbers represent normalized stress (normalized with yield stress). For this elastic case, the magnitude of the stresses is not important. Notice that the stresses

are negative ahead of the crack. For the illustration in Figure F.4b, the moment was applied in the opposite direction, i.e., an elbow opening moment. For this case, a low level of tension exists ahead of the crack tip despite the fact that the moment is attempting to close the crack faces.

The reason for this somewhat surprising behavior lies in the way that the elbow ovalizes due to bending moment. As seen, the closing moment ovalizes the elbow cross section into the shape of an oblate spheroid while the elbow opening moment causes a prolate spheroid deformed shape. The case illustrated in Figure F.4 represents a radius to thickness ratio, $R/t = 20$. The same behavior occurs for $R/t = 5$, i.e. the stiffer case. In fact, for the un-cracked case, an elbow closing moment results in compressive stresses that develop up to an angle of between 20 and 25 degrees at the toe of the elbow, depending on the R/t ratio.

This response is further summarized in Figure F.5. The top illustration summarizes the response to an elbow closing moment. As illustrated, this results in an oblate spheroid type ovalization. As illustrated, one can think of this ovalization as being caused by 'pinching' forces applied along a plane at the center of the crack. This type of ovalization will induce a compressive contribution to the stress state in this region. Hence, there is a competition between the crack closing caused by ovalization, and the opening caused by the global bending load. It turns out that this competition is won by the ovalization component for crack sizes less than 20 to 25 degrees, depending on R / t ratio.

For an elbow opening (or straightening) moment, bottom illustration in Figure F.5, the opposite occurs. The prolate type ovalization component causes crack opening while the global moment closes the crack. This leads to a modest crack opening for smaller crack sizes. Because of this, **circumferential cracks are not expected to develop at the knee of the elbow.** Rather, they are expected to develop for crack size angles on the order of 45 to 90 degrees. The solutions tabulated below are compiled for crack sizes of 45 and 90 degrees. For these larger crack sizes, the cracks are open along the entire length.

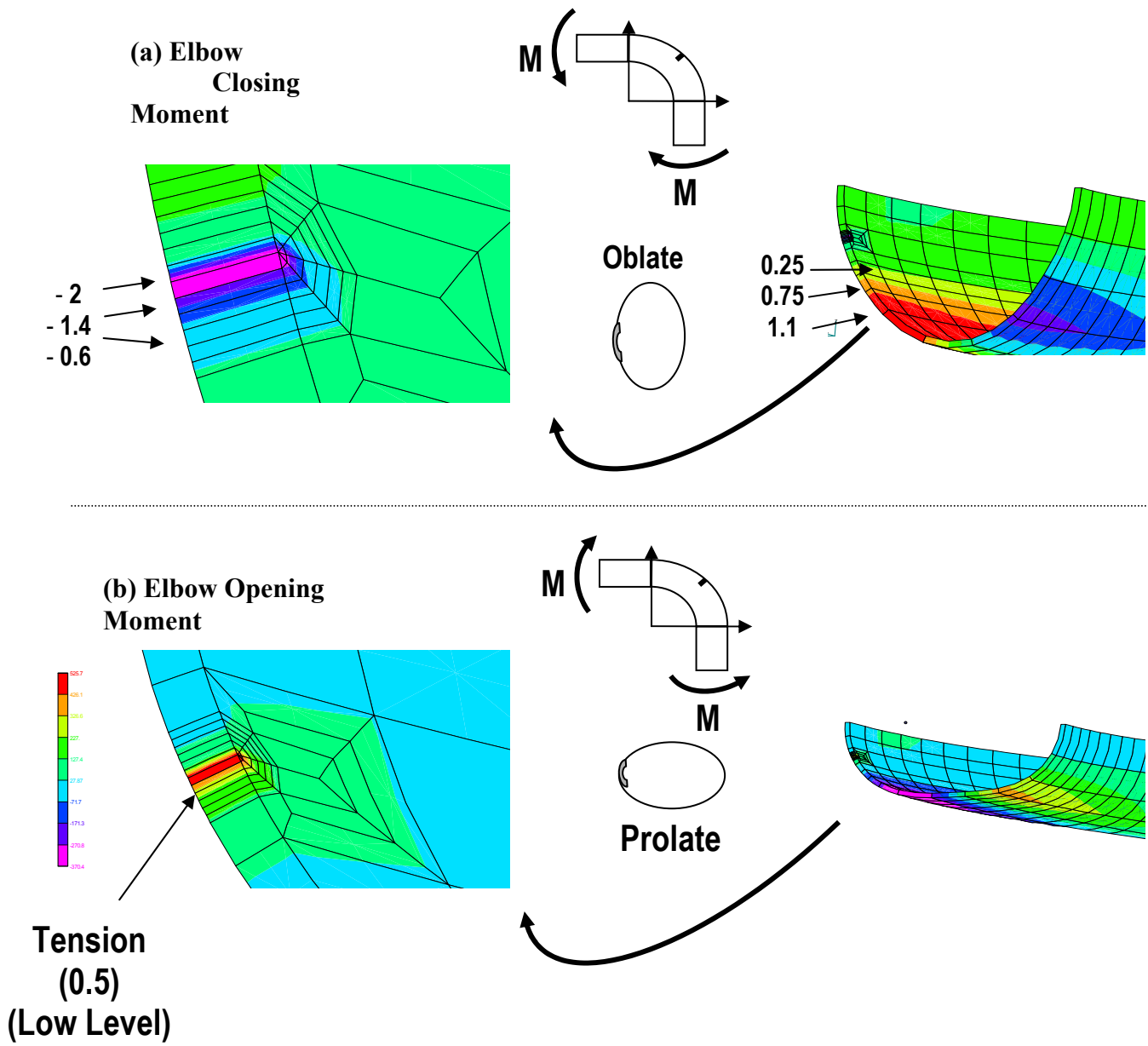


Figure F.4 Illustration of ovalization effects on stresses near the crack tip (Numbers represent crack opening stresses normalized with yield strength)

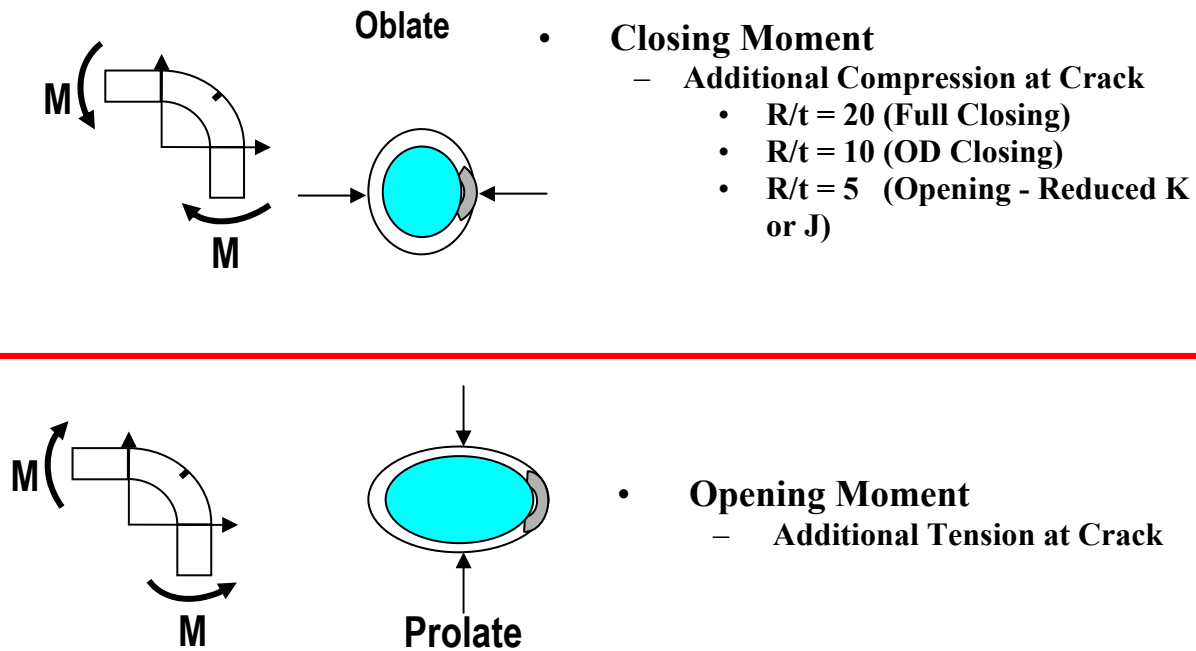


Figure F.5 Summary of ovalization effects on crack opening response of circumferential cracks in elbows subjected to bending

F.4.2 Axial Cracks

For the axial flank cracks the ovalization effect on crack opening is even more important. Figure F.6 illustrates the response of an axial flank crack, with total crack size angle of 15-degrees, subjected to bending. An elbow straightening moment causes tensile opening stresses in the crack region (this is also an elastic case).

The shaded contours on these plots represent the opening stress, σ_x , and all stress contours in the crack region are tensile. This means that the crack should open. However, it is also seen that

the ‘oblate’ spheroid ovalization causes the crack faces to rotate, with the inner crack opening greater than the outer diameter opening. The example illustrated in Figure F.6 is for the large R/t ratio case of 20. This same behavior occurs for the stiffer $R/t = 5$ case. In fact, for the 15-degree crack, the outer diameter region of the crack actually closes. Because of this crack face rotation, the crack opening functions were compiled for both the inner and outer surfaces. This ‘pinching’ of the crack opening along the outer surface should impede leaking, and hence LBB considerations. Hence, for LBB predictions one should account for crack face rotation in the leak rate models.

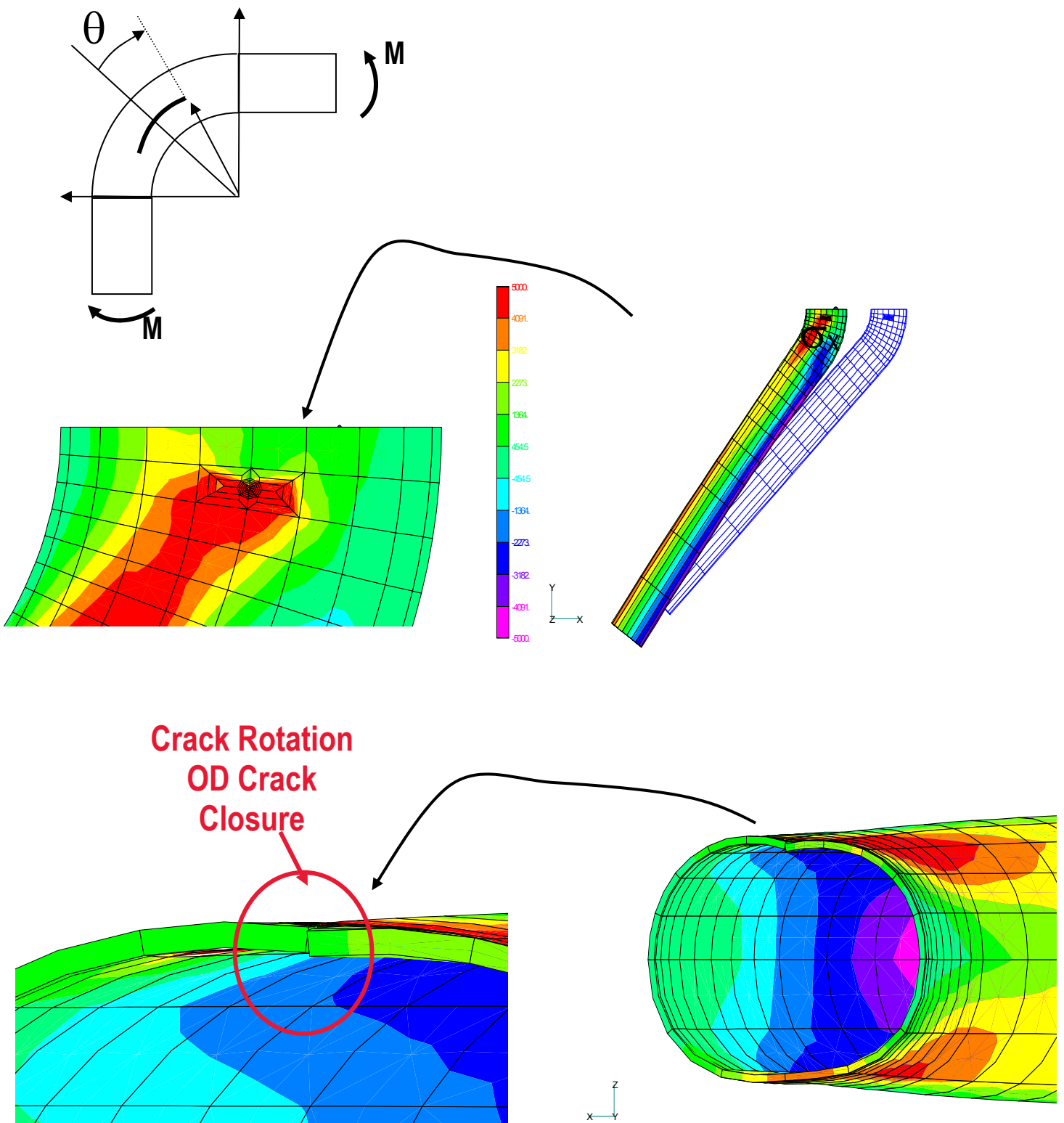


Figure F.6 Illustration of ovalization effects for 15-degree axial flank crack

Figure F.7 illustrates this effect further. Crack opening profile plots are illustrated for the outer diameter (OD), middle surface (MS), and along the inner diameter (ID) for an axial crack subjected to bending alone. In Figure F.7(a), which is for a 15-degree (total) crack angle (i.e. $2\theta = 15$ -degrees – see Figure F.1), the OD predicts negative crack opening. Of course, the negative crack openings are physically impossible, but it means that the crack faces will be closed and contacting each other at the OD. This will impede fluid leakage and affect leak rate calculations. Figure F.7(b) shows similar results for a 30-degree total crack angle. While the closure is not as severe as for the smaller crack, some crack face contact will occur along the OD. The predicted values in Figure F.7 are made assuming an elliptic crack opening shape. It is seen that elliptic profile is still a good approximation for the opening even if the crack faces rotate.

In an actual elbow, which is subjected to combined tension and pressure, the competition between the pressure, which causes opening COD's at both the ID and OD, and the bending, which closes the crack at the OD, will ultimately determine the service opening profile. However, the ovalization induced from elbow bending must be considered in the COD predictions which are then used in leak rate calculations for LBB considerations.

F.5 ESTIMATION SCHEMES

Elastic-plastic estimation schemes are based on the concept of proportional loading. If a cracked body is loaded in a proportional manner, such that the constitutive response is adequately modeled via deformation theory plasticity, then Illyushin has shown that deformations, stresses, and energies (e.g. J-integral) are proportional to a load parameter, material parameters, and geometric quantities. This concept has been overviewed extensively in the fracture mechanics literature (see for instance References F.1 through F.6).

For a cracked structure that obeys an elastic/power law constitutive relation, the stress/strain response follows:

$$\varepsilon = \varepsilon^e + \varepsilon^p = \frac{\sigma}{E} + k(\sigma)^n \quad (\text{F.2})$$

In Equation F.2, ε^e and ε^p are the elastic and plastic strains, E is the elastic modulus, and k and n are fitted material constants. This constitutive law leads to a violation of Illyushin's theorem since an elastic term is present (only the second term in Equation F.2 should be present). However, it has been observed that developing elastic-plastic estimation schemes using the separate elastic and plastic components provides a reasonable estimate for engineering purposes. It is common practice to write the constitutive relationship in the following form:

$$\frac{\varepsilon}{\varepsilon_0} = \frac{\sigma}{\sigma_0} + \alpha \left(\frac{\sigma}{\sigma_0} \right)^n \quad (\text{F.3})$$

where σ_0 is a reference stress, $\varepsilon_0 = \sigma_0 / E$, n is the fitted material parameter, and α is a material parameter related to k. The approximate solutions are determined by adding the contributions from an elastic and plastic part, as discussed next.

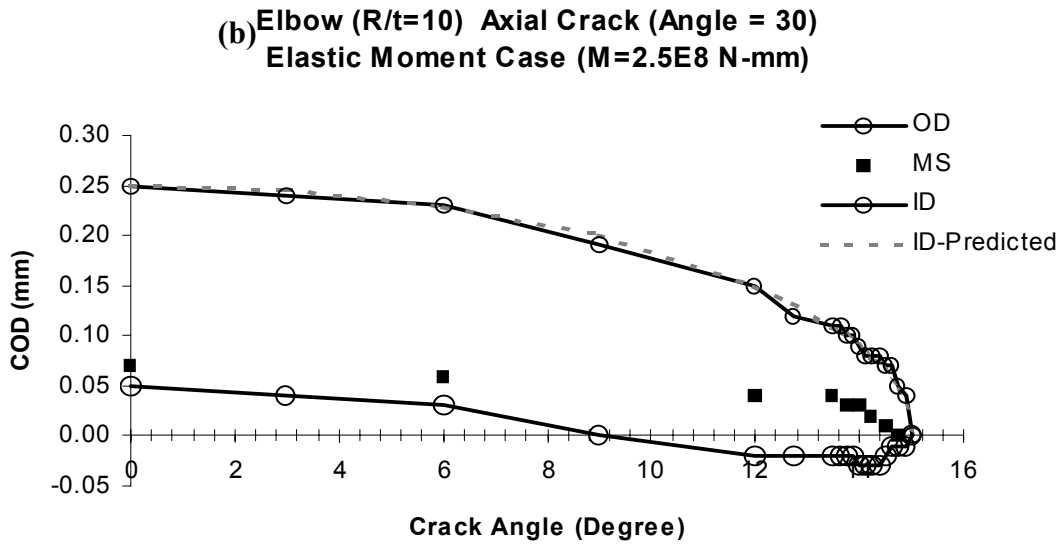
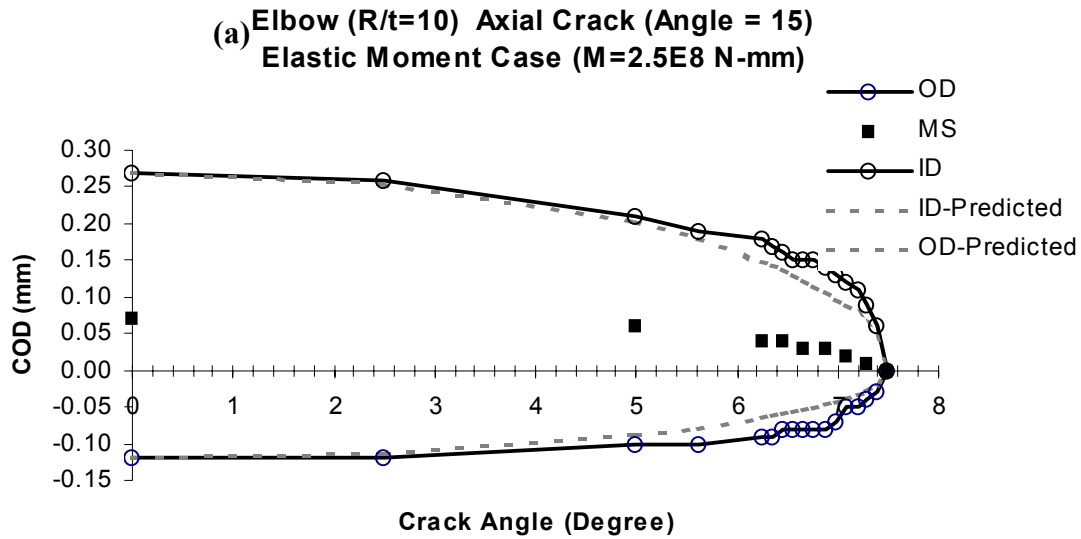


Figure F.7 Crack opening plots for axially cracked elbows – bending

F.5.1 Estimating J and Crack Opening Displacement (COD)

The estimation scheme for J is written as:

$$J = J^e + J^p \quad (F.4)$$

In Equation F.4, J represents the total estimated value for J, and J^e and J^p are the elastic and plastic components of J, respectively.

The estimation scheme for crack opening displacement is written as:

$$\delta_T = \delta^e + \delta^p \quad (\text{F.5})$$

In Equation F.5, δ_T is the total crack opening displacement at the mouth (i.e. displacement at the center of the crack), while δ_e and δ_p are the elastic and plastic contributions to the total COD, respectively.

F.5.2 Elastic Component J-Integral

The elastic component of J is estimated by superimposing the component contributions from the pressure (designated 'T' for 'Tension') and bending (designated 'B' for 'Bending'). This can be written as:

$$J^e = J_T^e + J_B^e = \frac{[F_T \sigma_T \sqrt{\pi a}]^2}{E} + \frac{[F_B \sigma_B \sqrt{\pi a}]^2}{E} = \frac{K_T^2 + K_B^2}{E} \quad (\text{F.6})$$

In Equation F.6, 'a' is crack size and F_T and F_B have been compiled in Tables F.1 to F.4 for the through-wall cracked elbow cases. The F_T functions were compiled by performing elastic solutions for the pure pressure case (with end cap tension present), and F_B functions were compiled for pure bending. σ_T and σ_B are calculated as nominal stresses using:

For Circumferential Cracks

$$\sigma_T = \frac{p(\pi R_i^2)}{\pi(R_o^2 - R_i^2)} \quad (\text{F.7})$$

For Axial Cracks

$$\sigma_T \equiv \sigma_H = \frac{2p(\pi R_i^2)}{\pi(R_o^2 - R_i^2)} \quad (\text{F.8})$$

Bending

$$\sigma_B = \frac{M(R_m)}{\frac{\pi}{4}(R_o^4 - R_i^4)} \quad (\text{F.9})$$

Here, p is the internal elbow pressure, R_i is inner radius, R_o is outer radius, R_m is mean radius, and M is the applied bending moment. The denominator in the bending stress definition is the moment of inertia. Notice that for the axial cracks, σ_T is defined as twice that for the circumferential crack, or a nominal σ_H since it is more like a 'hoop' stress that opens the axial cracks.

F.5.3 Elastic Component COD

Likewise, the elastic component of COD is estimated by superimposing the pressure (tension) and bending components of COD.

$$\delta_e = \delta_e^T + \delta_e^B \quad (\text{F.10})$$

where δ_e^T is the elastic COD contribution from pressure alone and δ_e^B is the elastic COD contribution from bending alone, and are written as:

$$\delta_e^T = \frac{4\sigma_T a}{E} V_1(T) \quad (\text{F.11})$$

$$\delta_e^B = \frac{4\sigma_B a}{E} V_1(B) \quad (\text{F.12})$$

The same definitions of the stress for the pressure loading apply, i.e., Equation F.7 is the tensile stress for circumferential cracks and Equation F.8 is the hoop stress used for axial cracks.

The functions $V_1(T)$ and $V_1(B)$ are compiled in Tables F.1 and F.2 for the circumferential crack cases and Tables F.3 and F.4 for the axial cracks. Notice from Tables F.3 and F.4 that $V_1(T)$ and $V_1(B)$ are tabulated for both the inside

and outside surfaces. Hence, the user can estimate the COD angle that occurs through the elbow wall as discussed in Section F.4. Figure F.8 illustrates this effect. The rotation through the elbow wall remains nearly linear, even when five parabolic elements are used to model the wall thickness.

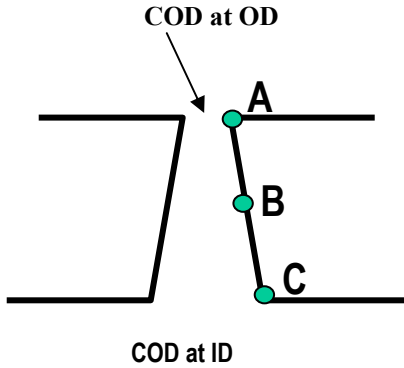


Figure F.8 Crack opening profile for axial cracks

F.5.4 Plastic Components of J

The plastic component of J is estimated as:

$$J^p = \alpha \sigma_0 \varepsilon_0 a (1 - \theta / \pi) h_1 (P / P'_0)^{n+1} \quad (\text{F.13})$$

Everything has been previously defined in Equation F.13 except P'_0 , which is defined as:

$$P'_0 = \frac{1}{2} \left[\frac{-\lambda P_0^2 R_m}{M_0} + \sqrt{\left\{ \frac{\lambda P_0^2 R_m}{M_0} \right\}^2 + 4P_0^2} \right] \quad (\text{F.14})$$

In Equation F.14, λ is the load ratio defined as:

$$\lambda = \frac{M}{PR_m} \quad (\text{F.15})$$

P in Equations F.13 and F.15 is defined as:

$$P = \sigma_T \pi (R_o^2 - R_i^2) \quad (\text{F.16})$$

It is emphasized that the h_1 functions from Equation F.13 have a strong dependence on load ratio, λ . Again as described above, σ_T is defined using Equation F.7 for circumferential cracks and using Equation F.8 for axial cracks. The two as yet undefined parameters in Equation F.14, M_0 and P_0 , are:

$$M_0 = 4\sigma_0 R_m^2 t [\cos(\theta/2) - 0.5 \sin(\theta)] \quad (\text{F.17})$$

For Circumferential Cracks

$$P_0 = 2\sigma_0 R_m t [\pi - \theta - 2 \sin^{-1}(0.5 \sin \theta)] \quad (\text{F.18a})$$

For Axial Cracks

$$P_0 = \sigma_0 R_m t [\pi - \theta - 2 \sin^{-1}(0.5 \sin \theta)] \quad (\text{F.18b})$$

Notice that, for the axial cracks the value of P_0 (Equation F.18b) is one half that for circumferential cracks. This is because hoop stresses dominate the failure for axial cracks, and hence P_0 should be smaller. Equation F.18a represents the standard limit load estimate for a circumferential crack in a pipe subjected to pressure. These definitions of P_0 lead to reasonable values for the h-functions that are easily interpolated to provide very accurate estimates between the values tabulated in Tables F.1 to F.4.

The values of h_1 are tabulated in Tables F.1 and F.2 for circumferential cracks and Tables F.3 and F.4 for axial cracks. They have been tabulated for values of $\lambda = [0, 0.5, 1.0, 2.0, 4.0, 8.0, \text{and infinity}]$. The case $\lambda = 0$ corresponds to the pure pressure case without bending, while $\lambda = \text{infinity}$ corresponds to the pure bending solution.

For typical nuclear piping LBB applications, the pipe experiences uniform or constant pressure the entire time while the moment is applied. As such, for a given crack size and material, the

only quantity that changes in the estimate for J in Equation F.13 is λ which continually increases as the moment increases, while P in Equation F.15 remains constant. The values of λ for which h_1 were tabulated are quite sufficient for practical nuclear applications. In fact, for practical purposes, a λ value of 18 should be used for interpolation when λ is between 8 and infinity. Most practical nuclear fracture assessments for pressurized elbows rarely find λ greater than about 6.

The compilations in Tables F.1 to F.4 represent 336 full nonlinear finite element solutions. These were compiled by proportionally applying the pressure and moment simultaneously. However, as will be seen in the validation section, solutions where pressure is applied first, followed by moment compare very well with the estimation scheme.

It is recommended that the plastic zone correction applied to the elastic solution be neglected. In general, as discussed in References F.1 to F.6, these type of J-estimation solutions have fundamental errors associated with them in the transition region between elastic and fully plastic solution ranges. However, we have found the plastic zone corrections to be unnecessary for most of the numerous validation cases that were performed (to be summarized later) here. However, the user can assure conservative solutions by including the form of the plastic zone correction procedure summarized on page 2-4 in Reference F.4. The user might want to use the plastic zone correction procedure for large 'n' values in cases where the elastic contribution to J is large (large crack size in high (R / t) elbow).

F.5.5 Plastic Components of COD

The plastic contribution to the crack opening displacement can be calculated using:

$$\delta^p = \alpha \varepsilon_0 a h_2 (P / P_0')^n \quad (F.19)$$

The h_2 -function is tabulated in Tables F.1 and F.2 for circumferential cracks and Tables F.3 and F.4 for axial cracks. The functions for the

axial cracks are tabulated for both the ID and OD so the user can estimate the variation of COD through the elbow thickness. As discussed above, the usual assumption of an elliptic crack opening shape works well for elbows even when the opening varies through the thickness. P in Equation F.19 is defined in Equations F.7 and F.16 for circumferential cracked elbows, and Equations F.8 and F.16 for axial cracks. P_0 is defined in Equation F.18a for circumferential cracks and Equation F.18b for axial cracks.

F.6 ESTIMATION SCHEME FOR PURE BENDING OF ELBOWS ($\lambda = \text{INFINITY}$)

For the $\lambda = \text{infinity}$ case, a bending moment only was applied. For this case, one can design the estimation scheme based on an alternative approach. The total estimate for J still uses Equation F.4 and Equation F.6, for the elastic estimate remains the same. Likewise, the total estimate for COD (Equation F.5) remains the same with Equations F.10 to F.12 providing the estimate for the elastic values. However, the estimates for J^p (Equation F.13) and δ^p (Equation F.19) can be replaced by:

$$J^p = \alpha \sigma_0 \varepsilon_0 a (1 - \theta / \pi) h_1^M (M / M_0)^{n+1} \quad (F.20)$$

$$\delta^p = \alpha \varepsilon_0 a h_2^M (M / M_0) \quad (F.21)$$

The compilations for h_1^M and h_2^M are provided in Tables F.5 and F.6. These can be compared directly with similar compilations for straight pipe to observe the differences.

Alternatively, all of the h-functions could have been based on formulas (Equations F.20 and F.21). It is instructive to investigate the choice made here to use Equations F.13 and F.19 rather than Equations F.20 and F.21. It will be seen that, in theory, one will obtain the same prediction of the plastic components of J and COD using either normalizing parameters, the choice made here results in much more accurate interpolation within the tables for predictions made for cases not directly tabulated.

First of all, from Figure F.9 the nature of the convergence of the h_1^M functions can be observed. The dashed horizontal line represents the converged solution of $h_1^M = 1.3$. This is for $R/t = 10$. The curve with the filled circles represents the convergence of the h-function versus load for a pure bending case (no internal pressure). The analyses were all performed using ABAQUS and the constitutive law represented by Equation F.2. Typically, the solution is monitored until the plastic strains become greater than ten times the elastic strains at every Gauss point in the body that is monitored. It is seen that it converges to the correct value at an M/M_0 value of about 5. Here, the monitoring procedure kept the analysis going until $M/M_0 = 15$. This was clearly adequate. In fact, convergence was assured for every value listed in Tables F.1 to F.4 in this fashion.

Also shown in Figure F.9 is a curve designated with solid diamonds. This was a case where a pressure of 10 MPa (typical operating pressure) was applied first, and then the bending moment was applied until it converged to the pure bending solution. With the definition of λ ($\lambda = M/(PR)$), since PR remains constant for this case (constant pressure), it is clearly seen that h_1^M depends on λ . As λ approaches infinity, the pure bending solution is obtained. This convergence to the pure bending solution occurs at large values of M/M_0 approaching 35. The h-functions published in Reference F.1 were developed in this way – pressure applied and held while the moment was applied. As such, the h-functions really are those for the pure bending case. Unfortunately, the h-functions obtained in this way are non-conservative and one will typically under predict the value of J – sometimes significantly, depending on λ .

Figure F.10 compares the h-functions calculated using Equations F.13 and F.20. The value of h based on Equation F.20 is very large for smaller values of λ (for instance, $h_1 = 3450$ for $\lambda = 0.5$). It is seen that the h-values based on Equation F.13 have much more uniform values. It should

be clear that the interpolation between values in the tables will be much more stable using the normalization based on Equation F.13 versus Equation F.20.

F.7 VALIDATION EXAMPLES

This next Section illustrates independent validation of the estimation schemes developed here. Before presenting the validation examples, it is useful to discuss the Ramberg-Osgood representation of material stress-strain data versus actual data. Figure F.11 illustrates a typical relationship. The bottom plot shows an example of idealized data that are to be fit with a Ramberg-Osgood equation. The ‘flow-2’ curve has an elastic slope and a yield stress of 200 MPa (29 ksi) in this case. The Ramberg-Osgood curve (Equation F.3) permits plastic strains to occur throughout the deformation. It is seen that, over the entire strain range, there is negligible difference between a Ramberg-Osgood and ‘flow’ representation (upper curve, Figure F.11). However, in the small strain regime, there are some small differences which manifest themselves as slight differences in predicted displacements, and J-Integral values. It will be seen that the representation in Figure F.11 results in a slightly conservative prediction of J-integral values in the following results. It is useful for the user of the estimation schemes to keep this in mind when making engineering predictions of fracture. How one fits a Ramberg-Osgood relation to actual test data can have an influence on predictions. See References F.5 and F.6 for more details.

In addition to the consistency checks on solution accuracy discussed above (see Figures F.9 and F.10), additional quality control was maintained by performing independent analyses. For each crack type and size, an independent analysis was performed for at least one set of material parameters and often for several sets. These validation analyses were performed as follows: pressure was applied first followed by bending. This violates the formal definition of a deformation theory solution. However, it is an excellent independent check on the accuracy of the solution procedure since, in actual nuclear piping, pressure is typically present, at constant

value, and then bending is applied. It will be seen that this results in slight differences between the flow theory solutions (which are strictly required for this set of loading conditions), and deformation theory solutions. For the examples which follow, the pressure applied was 5 MPa (0.75 ksi) for $R/t = 20$, 10 MPa (1.5 ksi) for $R/t = 10$, and 20 MPa (2.9 ksi) for the $R/t = 5$ cases. After the solution for pressure was complete, bending was applied. Solutions obtained in this manner are then directly compared to predictions using the estimation schemes developed here. The plastic-zone correction to the elastic solution are not included in the following.

F.7.1 Axial Cracks

Figures F.12 to F.14 illustrate the validation for some of the axial crack cases. It is clearly seen

that the estimation scheme is quite accurate, even for the flow theory cases. Notice that the crack opening displacement (COD) begins at a non zero value which corresponds the pressure case before applying a moment. Note also that the outer diameter (OD) COD's are typically much smaller than the ID cases. In fact, crack closure (Figure F.13) occurs for some cases.

F.7.2 Circumferential Cracks

Figures F.15 to F.17 illustrate the validation for some of the circumferential crack cases. Again, the estimation scheme performs very well. It is seen that there are some small differences between the deformation and flow theory solutions. However, in general, the deformation theory solution is more conservative and the estimation scheme typically falls between the two solutions.

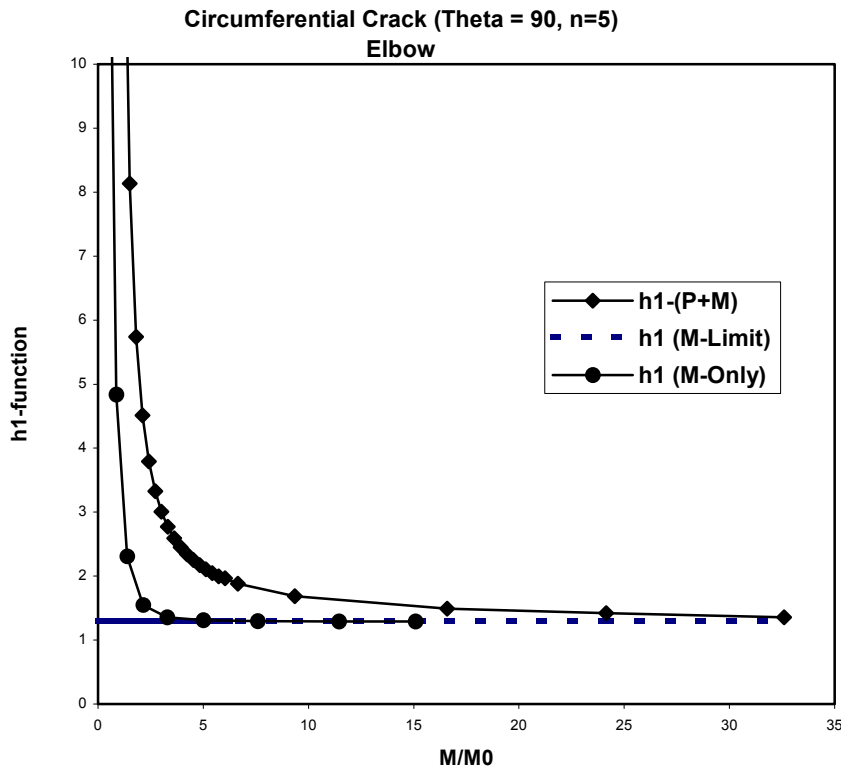


Figure F.9 Convergence of h-functions versus applied load

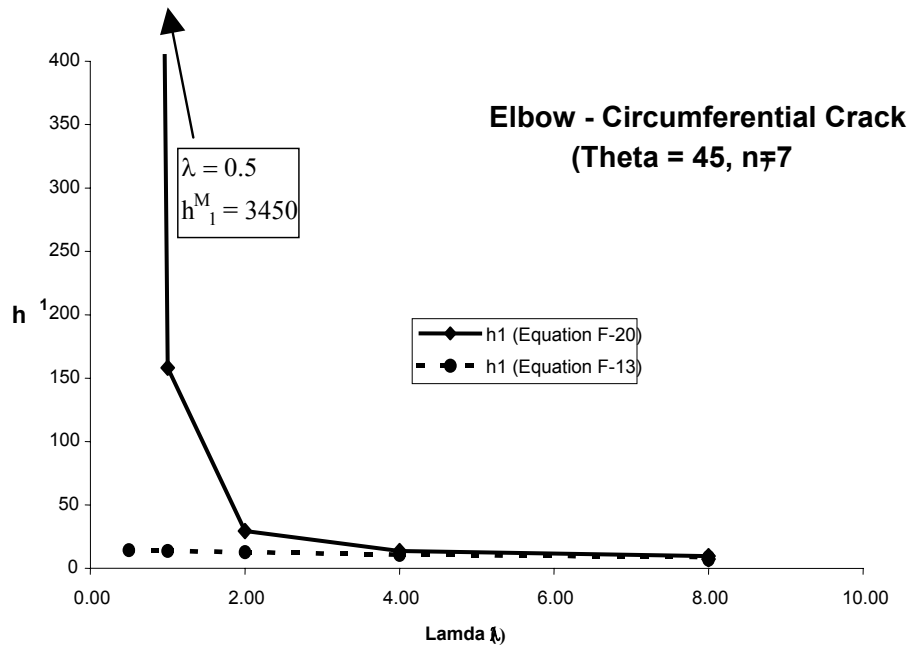


Figure F.10 Convergence of h-functions versus lambda

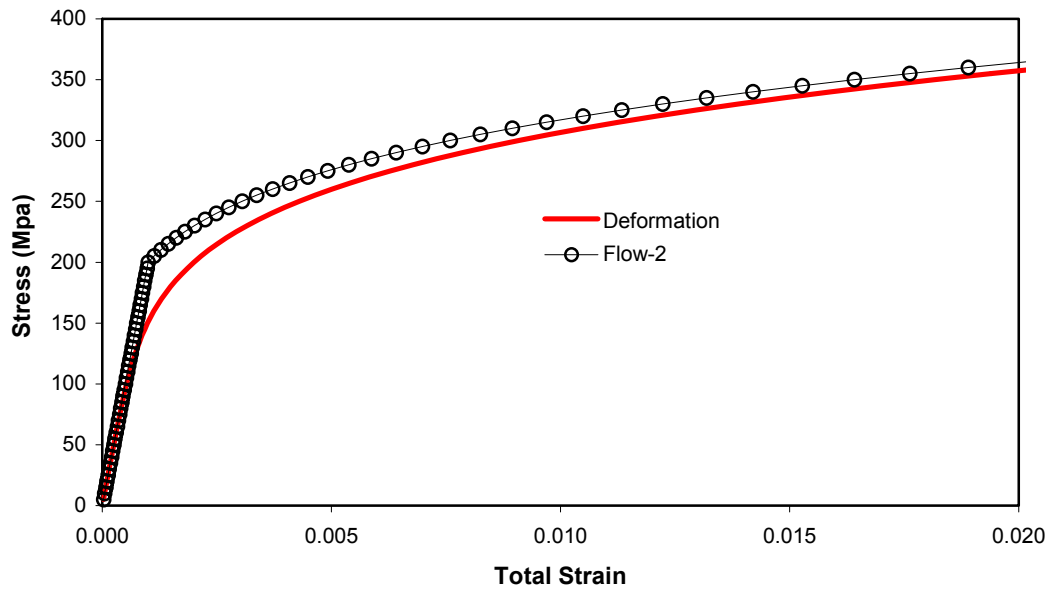
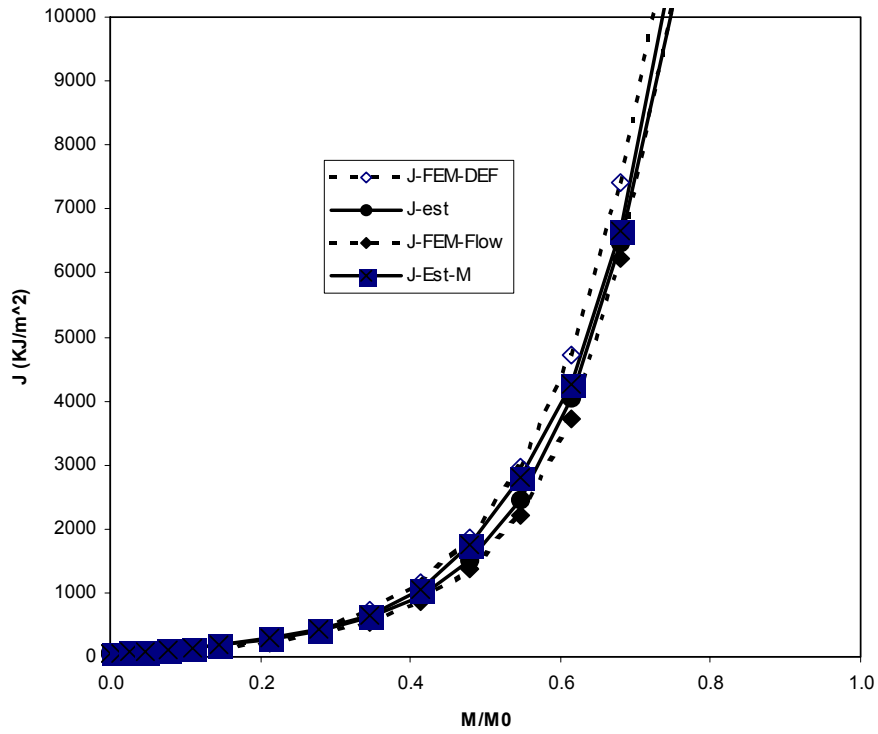


Figure F.11 Comparison between Ramberg-Osgood relationship and typical flow theory representation

Elbow - Axial Crack (Theta = 15, n=5, R/t=20)



Elbow - Axial Crack (Theta = 15, n=5, R/t=20)

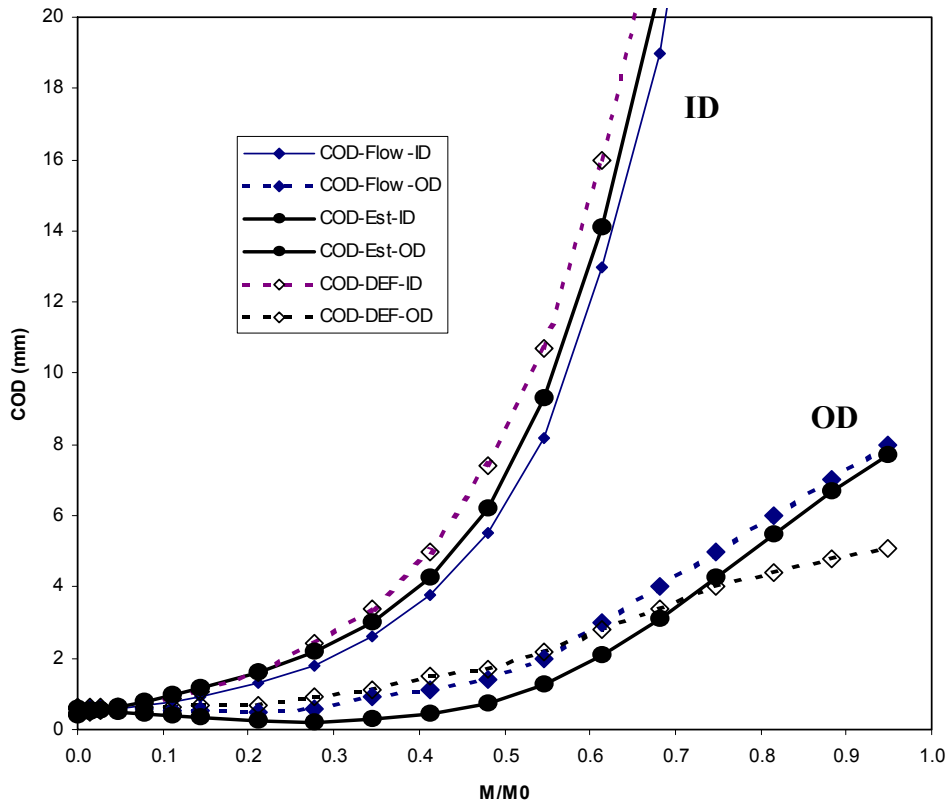
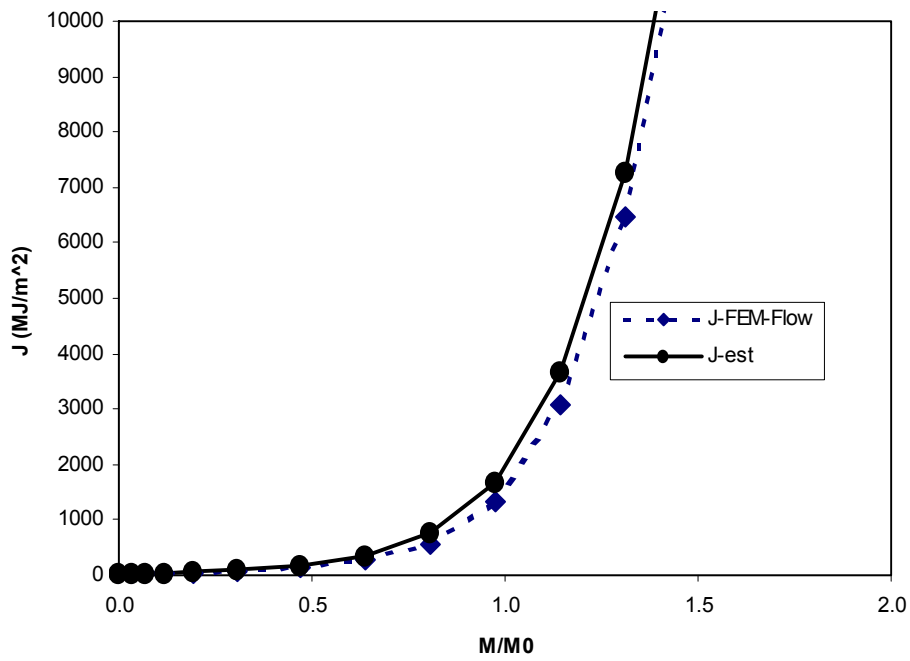


Figure F.12 Validation check (R/t = 20, axial crack $\theta = 15$ degrees, n = 5)



Elbow - Axial Crack (Theta = 15, n=5,R/t=5)

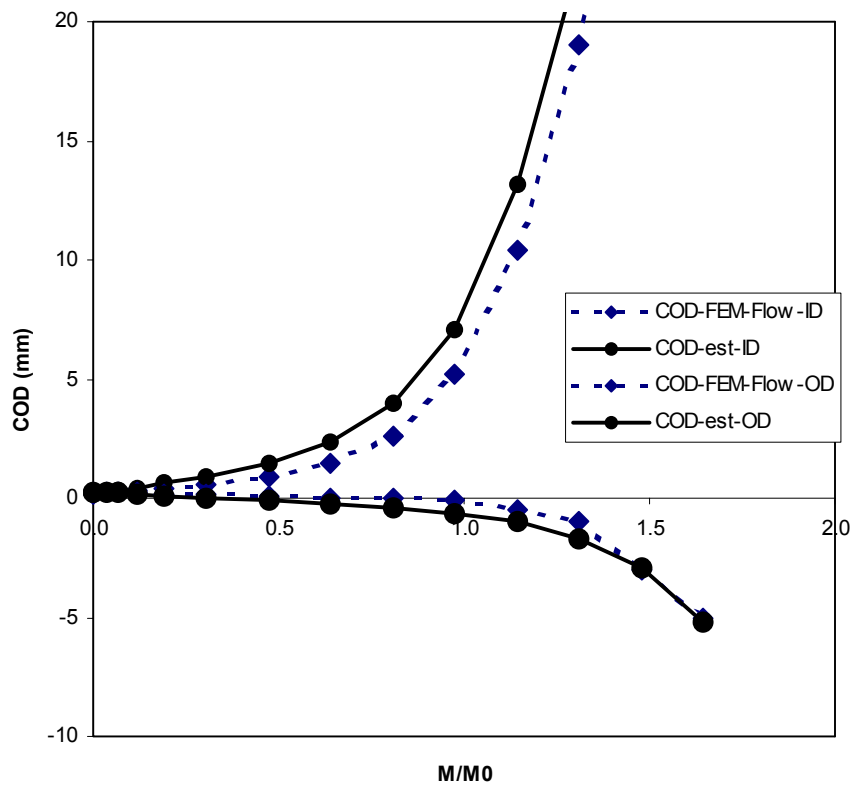


Figure F.13 Validation check (R/t = 5, axial crack, $\theta = 15$ degrees, n = 5)

Elbow - Axial Crack (Theta = 30, n=5, R/t=5)

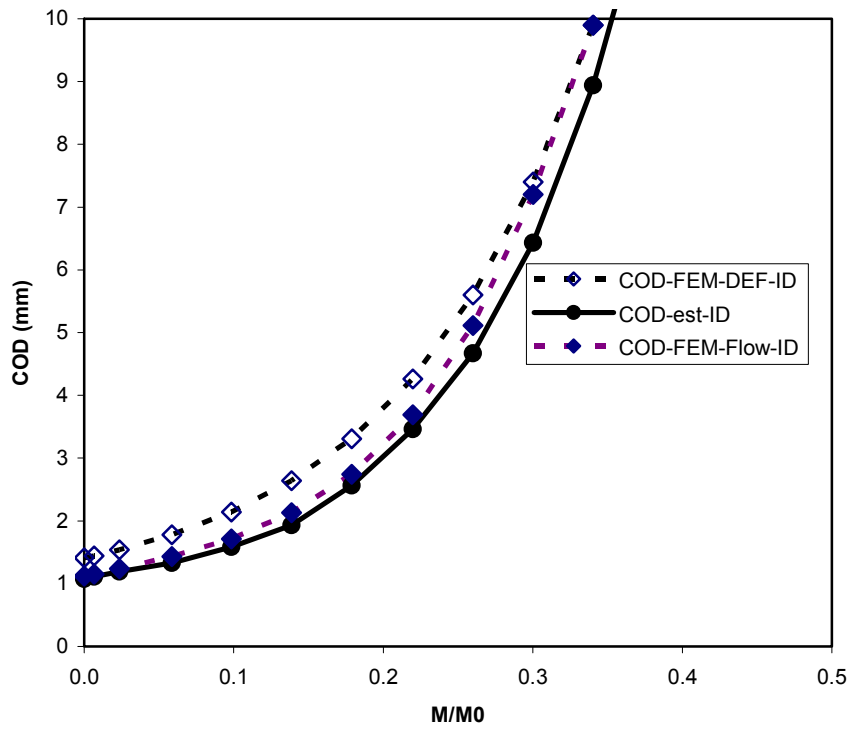
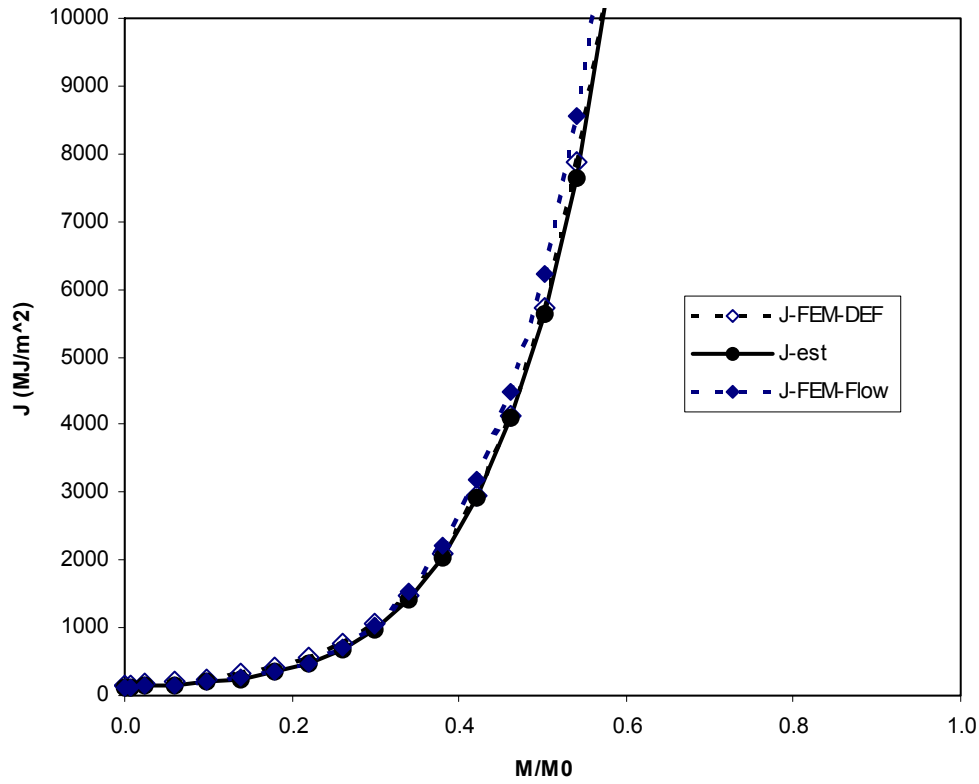


Figure F.14 Validation check (R/t = 5, axial crack, $\theta = 30$ degrees, n = 5)

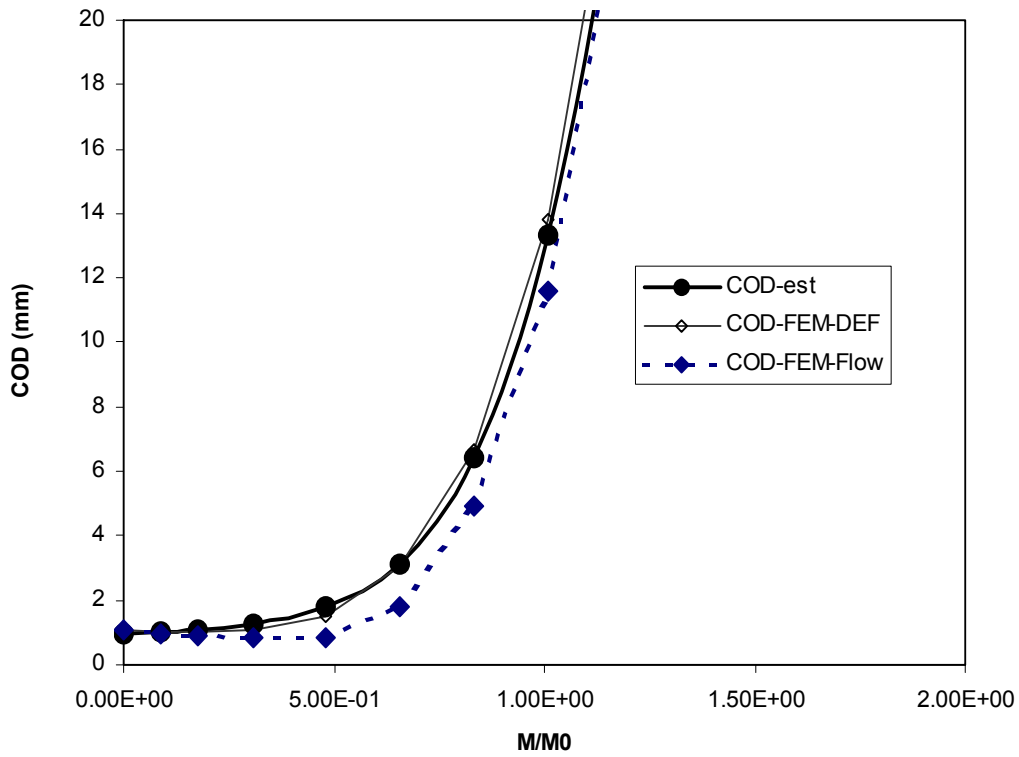
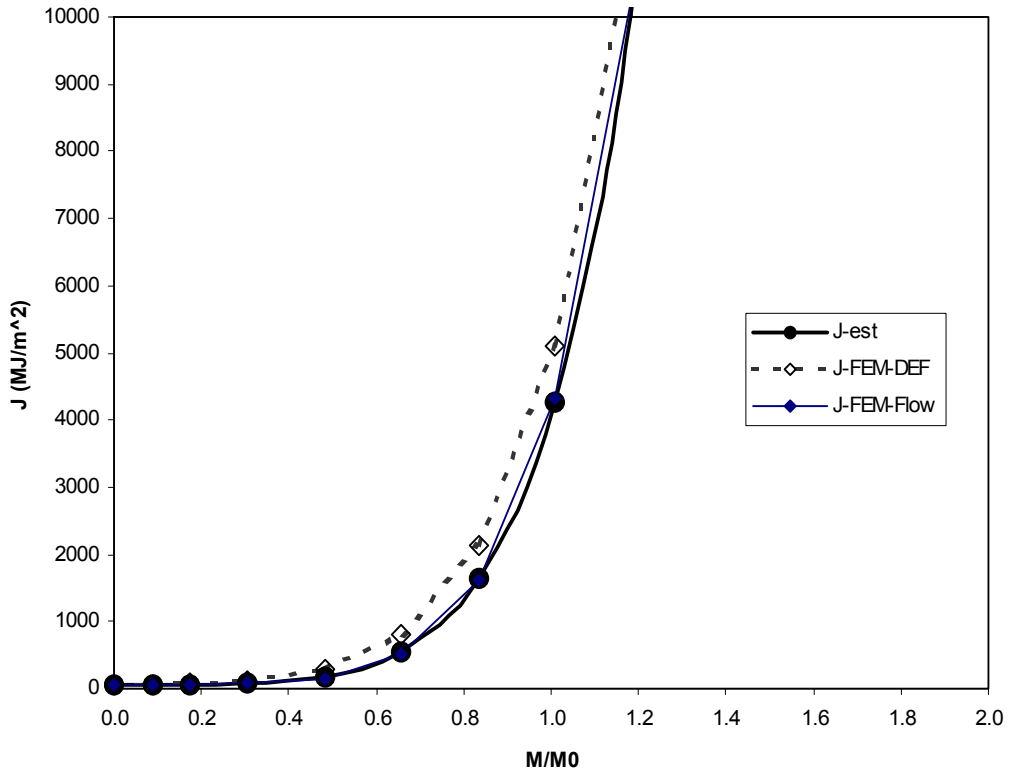


Figure F.15 Validation check ($R/t = 5$ circumferential crack, $2\alpha = 90$ degrees, $n = 5$)

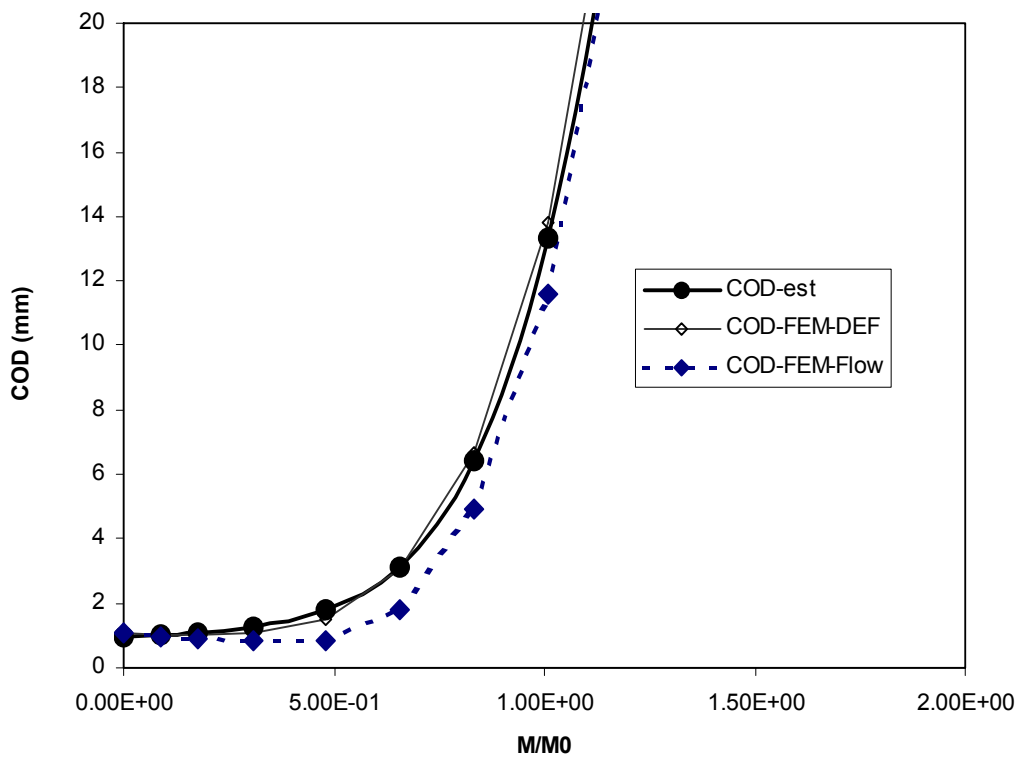
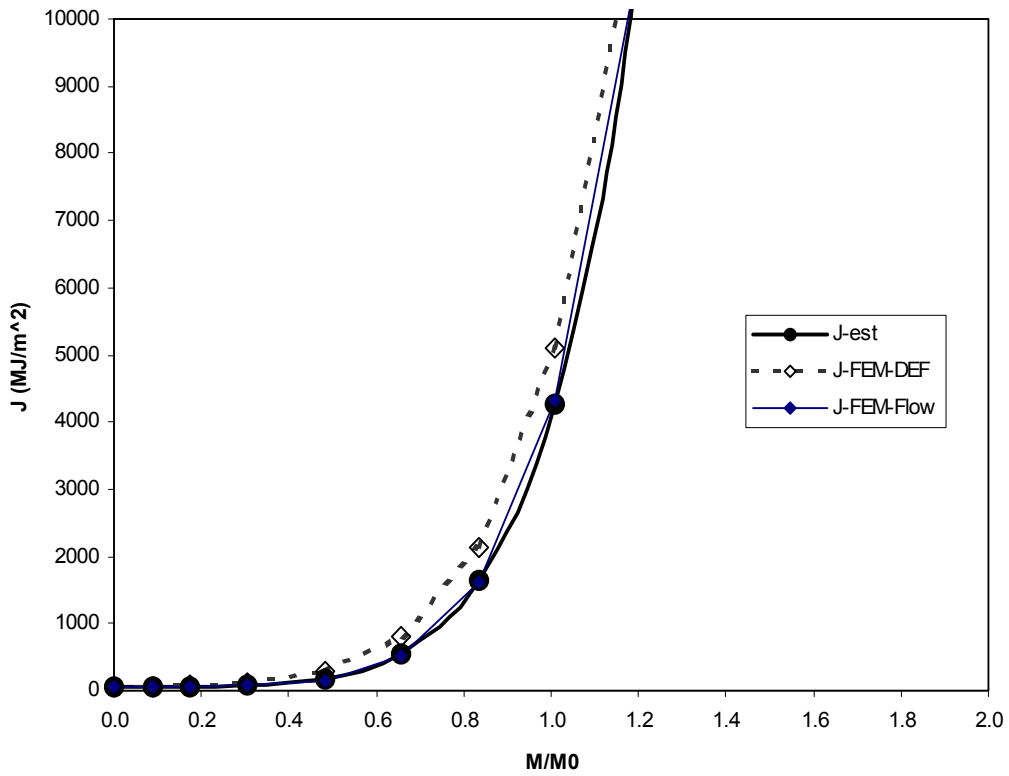
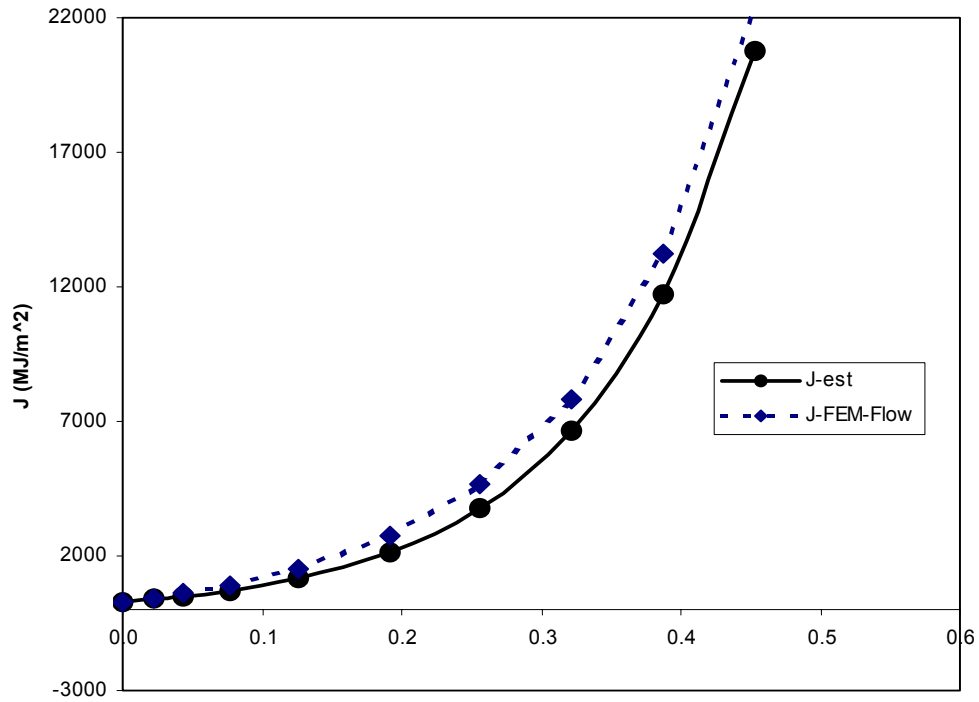


Figure F.16 Validation check ($R/t = 20$, circumferential crack, $2\alpha = 90$ degrees, $n = 5$)



Elbow - Circumferential Crack (Theta = 90, n=5, R/t=20)

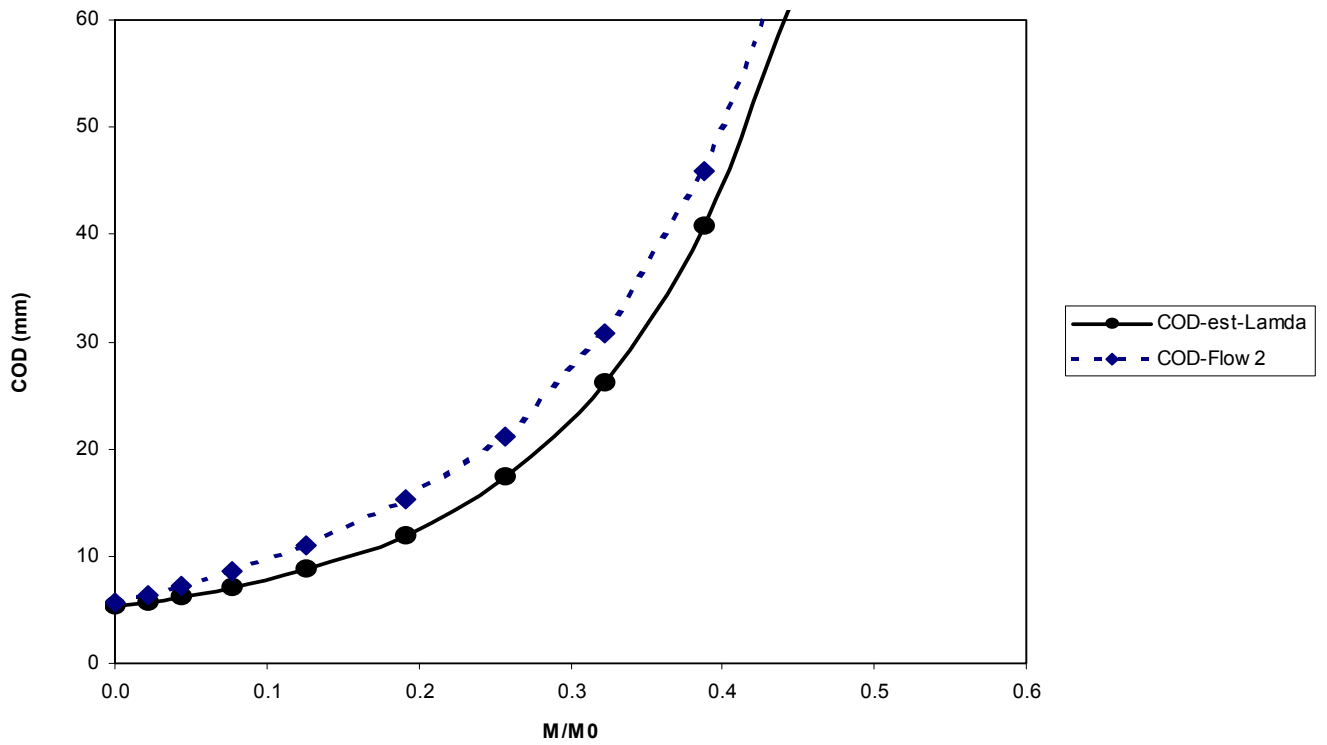


Figure F.17 Validation check (R/t = 20, circumferential crack, $2\theta = 180^\circ$, $\nu = 5$)

Table F.1 (a) Elbow with circumferential crack – combined pressure and bending compilation (R/t = 5, $\theta = 45^\circ$)

F-(T)	F-(B)	Lamda	n = 3	n = 5	n = 7	n = 10
			h₁	h₁	h₁	h₁
1.69	1.22	0.0	6.23	10.67	17.47	34.68
		0.5	6.39	8.04	9.75	12.42
		1.0	5.92	6.55	6.92	7.34
		2.0	5.23	5.10	4.78	4.25
		4.0	4.46	4.05	3.47	2.58
		8.0	3.91	3.43	2.79	2.01
		inf (=18)	3.17	2.76	2.11	1.36
		V-1 (T)	V-1 (B)	Lamda	h₂	h₂
h₂	h₂				h₂	h₂
2.04	1.19	0.0	8.59	14.87	24.65	49.31
		0.5	6.56	7.99	9.56	12.05
		1.0	5.70	6.17	6.45	6.78
		2.0	5.09	4.92	4.61	4.08
		4.0	4.59	4.17	3.57	2.67
		8.0	4.24	3.71	3.04	2.20
		inf (=18)	3.72	3.13	2.46	1.60

Table F.1(b) Elbow with circumferential crack – combined pressure and bending compilation (R/t = 10, $\theta = 45^\circ$)

F-(T)	F-(B)	Lamda	n = 3	n = 5	n = 7	n = 10
			h₁	h₁	h₁	h₁
2.16	0.87	0.0	10.55	17.79	28.26	53.93
		0.5	8.75	11.96	14.42	18.32
		1.0	8.46	11.86	13.60	16.54
		2.0	7.91	10.47	12.80	15.27
		4.0	6.83	9.06	10.76	12.08
		8.0	5.85	7.82	8.99	10.76
		inf (=18)	4.47	6.06	6.89	7.87
		V-1 (T)	V-1 (B)	Lamda	h₂	h₂
h₂	h₂				h₂	h₂
3.39	0.67	0.0	15.04	27.26	45.21	90.60
		0.5	9.17	12.29	14.89	19.01
		1.0	7.92	10.28	12.24	14.88
		2.0	7.45	9.61	11.60	13.82
		4.0	6.83	8.93	10.48	11.75
		8.0	6.18	8.21	9.37	11.09
		inf (=18)	5.07	6.89	8.06	8.86

**Table F.1(c) Elbow with circumferential crack – combined pressure and bending compilation
(R/t = 20, $\theta = 45^\circ$)**

			n = 3	n = 5	n = 7	n = 10
F-(T)	F-(B)	Lamda	h₁	h₁	h₁	h₁
3.01	0.25	0.0	21.04	33.34	46.65	61.68
		0.5	15.57	27.30	41.30	72.98
		1.0	13.48	26.87	44.95	88.46
		2.0	11.14	26.02	49.25	113.49
		4.0	7.82	21.81	44.90	115.15
		8.0	5.66	17.59	38.84	96.94
		inf (=18)	3.22	11.07	25.92	66.57
V-1 (T)	V-1 (B)	Lamda	h₂	h₂	h₂	h₂
6.30	0.66	0.0	33.70	54.86	81.83	112.34
		0.5	19.23	34.59	54.73	100.90
		1.0	14.06	26.80	44.28	86.08
		2.0	11.75	25.37	45.85	102.22
		4.0	8.95	24.18	47.14	114.72
		8.0	6.43	21.00	45.08	108.47
		inf (=18)	2.99	14.08	33.69	86.77

Table F.2 (a) Elbow with circumferential crack – combined pressure and bending compilation (R/t = 5, $\theta = 90^\circ$)

			n = 3	n = 5	n = 7	n = 10
F-(T)	F-(B)	Lamda	h₁	h₁	h₁	h₁
4.04	2.52	0.0	1.33	0.82	0.53	0.31
		0.5	2.30	1.77	1.53	1.29
		1.0	2.67	2.26	2.05	1.99
		2.0	2.59	2.08	1.82	1.64
		4.0	2.12	1.56	1.20	.90
		8.0	1.75	1.14	0.79	0.50
		inf (=18)	1.26	0.69	0.41	0.20

			h₂	h₂	h₂	h₂
V-1 (T)	V-1 (B)	Lamda	h₂	h₂	h₂	h₂
6.52	4.46	0.0	2.11	1.14	0.70	0.38
		0.5	2.92	2.08	1.72	1.42
		1.0	3.26	2.55	2.26	2.14
		2.0	3.21	2.43	2.07	1.83
		4.0	2.83	1.95	1.47	1.08
		8.0	2.49	1.53	1.04	0.65

Table F.2 (b) Elbow with circumferential crack – combined pressure and bending compilation (R/t = 10, $\theta = 90^\circ$)

			n = 3	n = 5	n = 7	n = 10
F-(T)	F-(B)	Lamda	h₁	h₁	h₁	h₁
4.16	3.24	0.0	1.99	1.00	0.62	0.36
		0.5	3.28	2.45	2.02	1.69
		1.0	4.04	3.23	2.88	2.68
		2.0	4.12	3.19	2.72	2.46
		4.0	3.53	2.46	1.88	1.38
		8.0	2.98	1.88	1.33	0.82
		inf (=18)	2.24	1.22	0.71	0.35

			h₂	h₂	h₂	h₂
V-1 (T)	V-1 (B)	Lamda	h₂	h₂	h₂	h₂
9.66	5.93	0.0	2.99	1.51	0.86	0.47
		0.5	4.25	2.92	2.30	1.85
		1.0	4.91	3.72	3.19	2.58
		2.0	4.05	3.78	3.12	2.74
		4.0	4.59	3.15	2.34	1.67
		8.0	4.09	2.57	1.77	1.06
		inf (=18)	3.35	1.84	1.06	0.50

**Table F.2 (c) Elbow with circumferential crack – combined pressure and bending compilation
(R/t = 20, $\theta = 90^\circ$)**

F-(T)	F-(B)	Lamda	n = 3	n = 5	n = 7	n = 10
5.00	4.56	0.0	h₁	h₁	h₁	h₁
		0.5	2.87	1.75	1.13	0.62
		1.0	6.27	4.93	4.21	3.36
		2.0	8.43	7.34	6.69	6.31
		4.0	9.34	8.28	7.64	6.90
		8.0	8.60	7.13	5.99	4.57
		inf (=18)	7.59	5.58	4.52	3.21
			5.95	3.96	2.69	1.55
F- (T)	F- (B)	Lamda	h₁	h₁	j₁	h₁
17.08	7.94	0.0	5.83	3.26	1.95	0.99
		0.5	8.27	6.31	5.22	4.03
		1.0	9.94	8.69	7.85	7.26
		2.0	10.72	9.85	9.16	8.25
		4.0	10.09	8.95	7.69	5.93
		8.0	9.13	7.32	6.12	4.44
		inf (=18)	7.57	5.57	3.96	2.35

**Table F.3 (a) Elbow with axial crack – combined pressure and bending compilation
(R/t = 5, $\theta = 15^\circ$)**

			n = 3	n = 5	n = 7	n = 10
F-(T)	F-(B)	Lamda	h₁	h₁	h₁	h₁
1.57	0.81	0.0	1.01	0.49	0.22	0.07
		0.5	0.73	0.28	0.10	0.02
		1.0	0.65	0.25	0.09	0.02
		2.0	0.59	0.24	0.09	0.02
		4.0	0.53	0.22	0.09	0.02
		8.0	0.46	0.19	0.07	0.02
		inf (=18)	0.33	0.12	0.04	0.01
Inner	Diameter					
V-1 (T)	V-1 (B)	Lamda	h₂	h₂	h₂	h₂
1.45	1.20	0.0	1.42	0.70	0.32	0.10
		0.5	1.49	0.59	0.21	0.04
		1.0	1.61	0.62	0.22	0.04
		2.0	1.76	0.73	0.27	0.06
		4.0	1.81	0.78	0.31	0.07
		8.0	1.68	0.72	0.29	0.07
		inf (=18)	1.30	0.51	0.19	0.04
Outer	Diameter					
V-1 (T)	V-1 (B)	Lamda	h₂	h₂	h₂	h₂
2.04	-0.45	0.0	2.40	1.22	0.58	0.18
		0.5	1.42	0.60	0.23	0.05
		1.0	0.96	0.41	0.16	0.03
		2.0	0.48	0.22	0.09	0.02
		4.0	0.09	0.06	0.03	0.01
		8.0	-0.15	-0.03	-0.01	-0.01
		inf (=18)	-0.37	-0.11	-0.04	-0.01

**Table F.3 (b) Elbow with axial crack – combined pressure and bending compilation
(R/t = 10, $\theta = 15^\circ$)**

			n = 3	n = 5	n = 7	n = 10
F-(T)	F-(B)	Lamda	h₁	h₁	h₁	h₁
1.79	1.26	0.0	1.44	0.78	0.41	0.15
		0.5	1.16	0.49	0.19	0.04
		1.0	1.20	0.56	0.23	0.06
		2.0	1.39	0.77	0.39	0.14
		4.0	1.56	0.97	0.57	0.25
		8.0	1.57	0.92	0.58	0.27
		inf (=18)	1.25	0.73	0.39	0.17
Inner V-1 (T)	Diameter V-1 (B)	Lamda	h₂	h₂	h₂	h₂
1.83	1.73	0.0	2.08	1.18	0.63	0.24
		0.5	2.28	0.99	0.39	0.08
		1.0	2.73	1.30	0.55	0.14
		2.0	3.53	2.06	1.08	0.40
		4.0	4.10	2.77	1.68	0.79
		8.0	4.15	2.76	1.81	0.89
		inf (=18)	3.39	2.23	1.28	0.59
Outer V-1 (T)	Diameter V-1 (B)	Lamda	h₂	h₂	h₂	h₂
2.59	-0.77	0.0	3.50	2.05	1.13	0.43
		0.5	2.28	1.12	0.48	0.11
		1.0	1.73	0.96	0.45	0.13
		2.0	0.98	0.70	0.41	0.17
		4.0	0.11	0.22	0.18	0.10
		8.0	-0.59	-0.21	-0.09	-0.03
		inf (=18)	-1.25	-0.64	-0.32	-0.13

**Table F.3 (c) Elbow with axial crack – combined pressure and bending compilation
(R/t = 20, $\theta = 15^\circ$)**

			n = 3	n = 5	n = 7	n = 10
F-(T)	F-(B)	Lamda	h₁	h₁	h₁	h₁
2.18	1.94	0.0	2.89	2.19	1.60	1.02
		0.5	2.46	1.37	0.67	0.22
		1.0	2.95	1.96	1.16	0.58
		2.0	4.21	3.59	2.87	2.04
		4.0	5.39	5.34	5.14	5.39
		8.0	5.60	5.82	6.44	6.91
		inf (=18)	4.71	4.81	4.54	4.59
Inner V-1 (T)	Diameter V-1 (B)	Lamda	h₂	h₂	h₂	h₂
2.68	2.64	0.0	4.47	3.65	2.78	1.90
		0.5	4.70	2.75	1.40	0.48
		1.0	4.72	4.25	2.61	1.31
		2.0	8.76	8.16	6.85	5.04
		4.0	11.00	12.27	12.62	13.66
		8.0	11.10	13.35	15.64	17.76
		inf (=18)	9.13	10.76	11.17	12.03
Outer V-1 (T)	Diameter V-1 (B)	Lamda	h₂	h₂	h₂	h₂
3.72	-1.04	0.0	7.08	3.91	4.65	3.15
		0.5	4.98	3.35	1.85	0.69
		1.0	4.33	3.57	2.40	1.30
		2.0	3.18	3.62	3.37	2.71
		4.0	1.11	3.00	2.58	3.10
		8.0	-0.95	-0.14	0.26	0.78
		inf (=18)	-3.14	-2.88	-2.62	-2.46

**Table F.4 (a) Elbow with axial crack – combined pressure and bending compilation
(R/t = 5, $\theta = 30^\circ$)**

			n = 3	n = 5	n = 7	n = 10
F-(T)	F-(B)	Lamda	h₁	h₁	h₁	h₁
2.18	0.79	0.0	2.32	1.67	1.20	0.83
		0.5	1.45	0.72	0.35	0.13
		1.0	1.07	0.45	0.18	0.05
		2.0	0.79	0.32	0.12	0.03
		4.0	0.56	0.22	0.08	0.02
		8.0	0.40	0.15	0.05	0.01
		inf (=18)	0.22	0.07	0.02	0.00
Inner V-1 (T)	Diameter V-1 (B)	Lamda	h₂	h₂	h₂	h₂
2.67	1.24	0.0	3.78	2.93	2.23	1.58
		0.5	2.80	1.49	0.76	0.29
		1.0	2.34	1.05	0.44	0.12
		2.0	2.34	1.05	0.44	0.12
		4.0	2.01	0.85	0.33	0.08
		8.0	1.68	0.69	0.26	0.06
		inf (=18)	0.96	0.33	0.11	0.02
Outer V-1 (T)	Diameter V-1 (B)	Lamda	h₂	h₂	h₂	h₂
3.87	0.16	0.0	6.35	4.90	4.03	2.91
		0.5	4.05	2.33	1.25	0.49
		1.0	2.90	1.38	0.60	0.16
		2.0	1.95	0.89	0.35	0.08
		4.0	1.21	0.52	0.21	0.05
		8.0	0.73	0.31	0.12	0.03
		inf (=18)	0.25	0.10	0.04	0.01

**Table F. 4 (b) Elbow with axial crack – combined pressure and bending compilation
(R/t = 10, $\theta = 30^\circ$)**

			n = 3	n = 5	n = 7	n = 10
F-(T)	F-(B)	Lamda	h₁	h₁	h₁	h₁
2.58	1.22	0.0	4.26	4.35	4.70	5.88
		0.5	2.64	1.73	1.22	0.80
		1.0	2.18	13.16	0.62	0.24
		2.0	1.95	1.11	0.59	0.22
		4.0	1.67	0.99	0.57	0.24
		8.0	1.37	0.80	0.19	0.20
		inf (=18)	0.88	0.47	0.24	0.09
Inner V-1 (T)	Diameter V-1 (B)	Lamda	h₂	h₂	h₂	h₂
4.13	2.01	0.0	8.48	9.81	11.35	14.96
		0.5	5.99	4.48	3.41	2.40
		1.0	5.21	3.12	1.78	0.67
		2.0	4.93	3.03	1.68	0.62
		4.0	4.61	2.91	1.75	0.76
		8.0	4.05	2.54	1.52	0.69
		inf (=18)	2.91	1.68	0.90	0.34
Outer V-1 (T)	Diameter V-1 (B)	Lamda	h₂	h₂	h₂	h₂
5.64	0.40	0.0	12.92	15.37	18.03	23.83
		0.5	8.21	6.59	5.20	3.16
		1.0	6.27	4.01	2.38	0.87
		2.0	4.81	3.12	1.77	0.70
		4.0	3.48	2.34	1.87	0.64
		8.0	2.39	1.64	1.02	0.48
		inf (=18)	1.00	0.67	0.38	0.15

**Table F. 4 (c) Elbow with axial crack – combined pressure and bending compilation
(R/t = 20, $\theta = 30^\circ$)**

			n = 3	n = 5	n = 7	n = 10
F-(T)	F-(B)	Lamda	h₁	h₁	h₁	h₁
3.13	1.91	0.0	9.38	15.32	27.79	79.02
		0.5	5.87	5.53	6.71	9.57
		1.0	5.51	4.46	3.55	2.68
		2.0	5.96	5.13	4.35	3.43
		4.0	5.96	6.14	6.07	2.95
		8.0	5.33	5.61	5.89	5.68
		inf (=18)	3.64	3.47	3.23	3.03
Inner V-1 (T)	Diameter V-1 (B)	Lamda	h₂	h₂	h₂	h₂
6.78	3.64	0.5	22.16	41.11	79.18	233.37
		1.0	15.12	17.82	22.37	16.14
		2.0	14.03	13.13	11.61	9.62
		4.0	14.72	14.20	12.74	10.53
		8.0	14.96	16.90	17.65	17.73
		inf (=18)	13.76	16.00	17.75	18.10
		inf (=18)	9.95	10.57	10.48	10.29
Outer V-1 (T)	Diameter V-1 (B)	Lamda	h₂	h₂	h₂	h₂
8.71	1.36	0.0	28.07	57.82	111.73	329.87
		0.5	19.34	24.05	30.95	15.74
		1.0	16.16	15.95	14.60	12.49
		2.0	14.43	14.48	13.25	11.15
		4.0	12.42	14.78	15.70	16.00
		8.0	9.74	12.18	13.97	14.47
		inf (=18)	5.20	6.03	6.20	6.29

Table F.5 Elbow with circumferential crack – pure bending compilation ($\theta = 45, 90^\circ$) for use with Equations E.19 and E.20

(a) $R/t = 5$, (b) $R/t = 10$, (c) $R/t = 20$

(a)

	n = 3	n = 5	n = 7	n = 10
θ	h_1	h_1	h_1	h_1
45.0	3.27	2.89	2.24	1.47
90.0	1.31	0.73	0.44	0.22
θ	h_2	h_2	h_2	h_2
45.0	3.81	3.25	2.60	1.72
90.0	2.05	1.08	0.64	0.32

(b)

	n = 3	n = 5	n = 7	n = 10
θ	h_1	h_1	h_1	h_1
45.0	4.61	6.34	7.32	8.55
90.0	2.32	1.29	0.77	0.38
θ	h_2	h_2	h_2	h_2
45.0	5.18	7.16	8.49	9.55
90.0	3.45	1.93	1.13	0.55

(c)

	n = 3	n = 5	n = 7	n = 10
θ	h_1	h_1	h_1	h_1
45.0	3.32	11.58	27.53	72.32
90.0	6.18	4.20	2.91	1.72
θ	h_2	h_2	h_2	h_2
45.0	3.06	14.62	35.51	93.56
90.0	7.79	5.84	4.24	2.58

Table F.6 Elbow with axial crack – pure bending compilation ($\theta = 15, 30^\circ$) for use with Equations E.19 and E.20

(a) $R/t = 5$, (b) $R/t = 10$, (c) $R/t = 20$

(a)

	n = 3	n = 5	n = 7	n = 10
θ	h_1	h_1	h_1	H_1
15.0	5.8	9.1	13.6	22.8
30.0	4.0	5.6	7.5	11.4
Inner Diameter				
θ	h_2	h_2	h_2	h_2
15.0	11.2	18.5	28.4	49.4
30.0	8.3	12.0	16.5	25.8
Inner Diameter				
θ	h_2	h_2	h_2	h_2
15.0	-3.2	-4.1	-5.6	-8.7
30.0	2.1	3.6	5.4	9.0

(b)

	n = 3	n = 5	n = 7	n = 10
θ	h_1	h_1	h_1	h_1
15.0	22.1	54.6	123.0	467.5
30.0	15.5	35.4	76.5	240.1
Inner Diameter				
θ	h_2	h_2	h_2	h_2
15.0	29.2	80.8	195.8	777.9
30.0	25.1	61.3	138.6	457.0
Inner Diameter				
θ	H_2	h_2	h_2	h_2
15.0	-10.8	-23.1	-49.5	-176.30
30.0	8.7	24.5	58.8	205.6

(c)

	n = 3	n = 5	n = 7	n = 10
θ	h_1	h_1	h_1	h_1
15.0	83.4	358.0	1422.8	12395.0
30.0	64.6	259.4	1017.9	8254.8
Inner Diameter				
θ	h_2	h_2	h_2	h_2
15.0	78.8	390.7	1705.8	15853.2
30.0	86.1	385.3	1609.4	13664.0
Inner Diameter				
θ	H_2	h_2	h_2	h_2
15.0	-27.1	-104.5	-400.8	-3240.7
30.0	45.0	219.7	951.6	8350.6

F.8 SIMPLIFIED ANALYSIS FOR THROUGH-WALL CRACKS IN ELBOWS

To establish a more complete Regulatory Guide for Leak-Before-Break, an evaluation procedure for through-wall cracks in elbows was desired. Finite element solutions for elbows with axial and circumferential cracks under combined pressure and bending have been developed as discussed above. This effort was somewhat similar to the work done for surface cracks in NUREG/CR-6444, "Fracture Behavior of Circumferentially Surface-Cracked Elbows" that was done for the IPIRG-2 program, Ref. F.14.

The recent through-wall-cracked elbow work developed a limited number of finite element solutions and a J-estimation scheme with h-function fits through these solutions. As with the case of the prior surface-cracked elbow work, it was desirable to see if a simplified solution could be developed from these results and be applicable over a wider range of through-wall cracks in elbows.

F.8.1 Finite Element Analyses

As discussed above, numerous 3-D finite element analyses were developed for the intent of developing a J-estimation scheme analyses. In developing these analyses, there were a limited number of analyses that could be conducted. The analyses conducted were for:

- Axial (flank) cracks with two crack lengths,
- Circumferential (extrados) cracks with two crack lengths,
- Elbows with two different cross-sectional radius-to-thickness (R/t) ratios,
- 90-degree, long-radius elbows,
- Materials with several different strain-hardening exponents, and
- Combined internal pressure and bending.

The initial finite element analyses were made with a constant pressure and varying the bending moment. For the estimation scheme developed, additional analyses were conducted where the pressure was varied in proportion to the bending moment. In the constant pressure cases, the

pressure was fixed so that the hoop stress corresponded to the average design stress (S_m) of nuclear pipe materials. From NUREG/CR-6445, this S_m value was estimated to be 122.5 MPa (17.7 ksi), Ref. F.1.

For the purpose of evaluating an estimation procedure, the constant pressure elbow finite element results were used directly, rather than using the estimation procedure.

The cases chosen to evaluate were:

- The longest and shortest crack lengths,
- Both axial and circumferential crack orientations, and
- The largest and smallest cross-sectional R/t ratios.

Since most nuclear pipe materials have strain-hardening exponents of about 5, only that case was examined. Thus, the extreme eight cracked elbow cases were examined.

F.8.2 Simplified Procedures

In NUREG/CR-6444, a simplified procedure was developed for surface cracks in elbows, Ref. F.14. This involved comparing the elbow results to those for a circumferential surface crack in a pipe of the same dimensions and with the same material properties.

From that report, it was found that the ratio of the pipe to the elbow moments at the same J value was constant as the J value increased. This constant ratio between the elbow and pipe moment values for a particular case was found to be theoretically correct when comparing the general equations for fully plastic solutions for straight pipes and elbows as given below:

$$J^{pipe} = \alpha \sigma_0 \varepsilon_0 b h_1^{pipe} (M^{pipe} / M_0^{pipe})^{n+1} \quad (F.22a)$$

$$J^{elbow} = \alpha \sigma_0 \varepsilon_0 b [R_m / (\lambda_1 t)] h_1^{elbow} (M^{elbow} / M_0^{elbow})^{n+1} \quad (F.22b)$$

where,

$\alpha, \sigma_o, \epsilon_o, n$ = Ramberg-Osgood parameters
 $h_1^{\text{pipe}}, h_1^{\text{elbow}}$ = FEM determined geometric parameters relating moment to J
 $M_o^{\text{pipe}}, M_o^{\text{elbow}}$ = reference moments at a stress of σ_o
 $b = t - a$
 t = thickness
 λ_1 = an elbow parameter = $R_{el}t/R_m^2$
 R_{el} = bend radius of the elbow
 R_m = mean radius of pipe and elbow

Considering the case where $J^{\text{pipe}} = J^{\text{elbow}}$, for the same material, pipe size, and crack size gives

$$h_1^{\text{pipe}} (M^{\text{pipe}}/M_o^{\text{pipe}})^{n+1} |_{J} = h_1^{\text{elbow}} [R_m/(\lambda_1 t)] (M^{\text{elbow}}/M_o^{\text{elbow}})^{n+1} |_{J} \quad (\text{F.23})$$

Rearranging Equation F.23 gives

$$(M^{\text{pipe}}/M^{\text{elbow}}) |_{J} = [(h_1^{\text{elbow}}/h_1^{\text{pipe}})^{1/(n+1)} [R_m/(\lambda_1 t)]^{1/(n+1)} (M_o^{\text{pipe}}/M_o^{\text{elbow}})] |_{J} \quad (\text{F.24})$$

For a given material, pipe, and elbow geometry and similar crack size, the right-hand side of Equation F.24 is a constant and independent of the J value, and hence $(M^{\text{pipe}}/M^{\text{elbow}}) |_{J}$ is a constant. The plastic part of J dominates the moment ratio for J_{applied} values of generally greater than 100 kJ/m² (570 in-lb/in²), which bounds the toughness range of typical nuclear piping materials, except perhaps some aged CF8M steels. It was then found that the constant value for the particular crack-size/pipe radius-to-thickness geometry/material case varied linearly with the elbow stress indices, B_2 . This same simplified approach was examined for through-wall cracks in elbows as part of this effort.

F.8.2.1 Straight-Pipe Solutions - For the relative comparison of the moment versus J solutions of the straight pipe to the elbow cases, two different circumferential through-wall-cracked straight-pipe solutions were used. These were the LBB.ENG2 and original GE/EPRI methods in Version 3.0 of NRCPIPE.

The LBB.ENG2 method was used since it was the most accurate in predicting the maximum moment for through-wall-cracked straight-pipe

experiments, Ref. F.9. However, the LBB.ENG2 analysis requires an additional parameter that was not used in the FE solutions, that is, the ultimate strength of the material. For this analysis procedure it was assumed that the yield to-ultimate strength ratio was 0.85.

The GE/EPRI solution does not need the ultimate strength of the material, so it was also used. However, it was experimentally found that the GE/EPRI analysis was the most conservative analysis in predicting the full-scale straight-pipe experiments, i.e., it overpredicted the crack-driving force, Ref. F.9.

All analyses were for 410-mm (16.14-inch) outside diameter pipe. Additionally, all analyses were conducted with non-growing cracks.

F.8.2.2 Comparison of Circumferential Extrados Through-Wall-Cracked Elbow and Straight-Pipe Solutions

- To make this comparison, the J versus moment curves from both the straight pipe and elbow solutions were first compared. Figures F.18 and F.19 show the results for the circumferential crack case with an R/t of 20 and total crack lengths of 90 and 180 degrees. Note in Figure F.18 that there is also a curve for an elbow curve-fit equation. This was done since the pipe and elbow solutions did not have values at exactly the same J values. The elbow curve-fit equation (as shown in Figure F.18) was used to compare the moments of the elbow to the straight pipe at the same J values, i.e., for $(M^{\text{pipe}}/M^{\text{elbow}}) |_{J}$.

Figure F.18 shows that the curve fit is a very close approximation of the FE data points. Also, there is a difference in the two straight-pipe solutions, with the GE/EPRI solution giving higher J-values as was expected.

In Figure F.19, it is interesting to note that the elbow and LBB.ENG2 straight-pipe analyses give similar results, whereas the GE/EPRI solution for the straight pipe gives much higher J values. After these analyses were completed, it was recalled that the 180-degree crack R/t=20 analysis in the GE/EPRI solution in NRCPIPE was found to be in error, so that in this case only the LBB.ENG2 analysis should be used.

The results for the $R/t = 5$ case are shown in Figures F.20 and F.21.

value versus the moment ratio is given for each case in Figures F.22 to F.25.

The next step was to compare the ratio of the moments at the same J value. A graph of the J

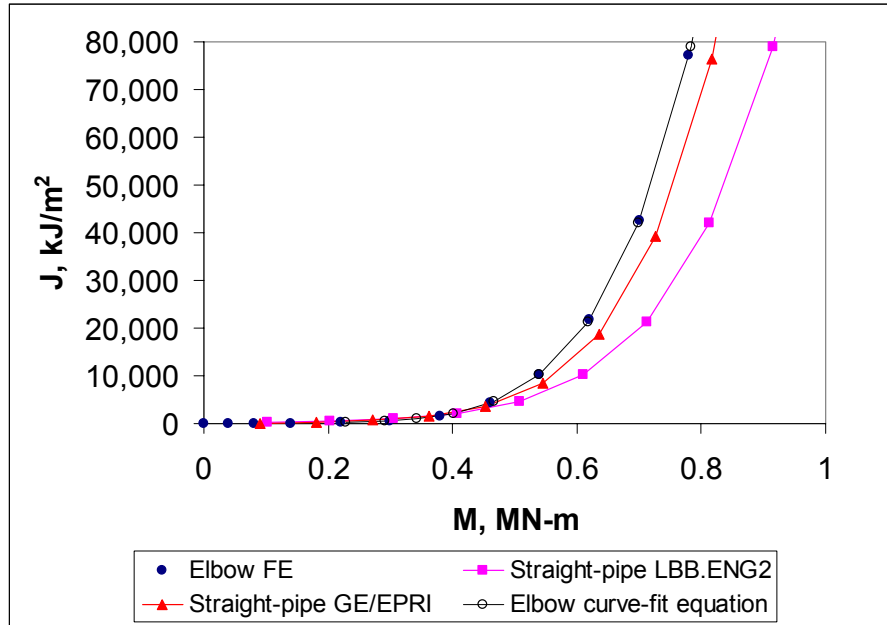


Figure F.18 Comparison of J versus moment curves for a circumferential through-wall crack in a straight pipe and centered on the extrados of an elbow with an $R/t = 20$ and $2\theta = 90$ degrees

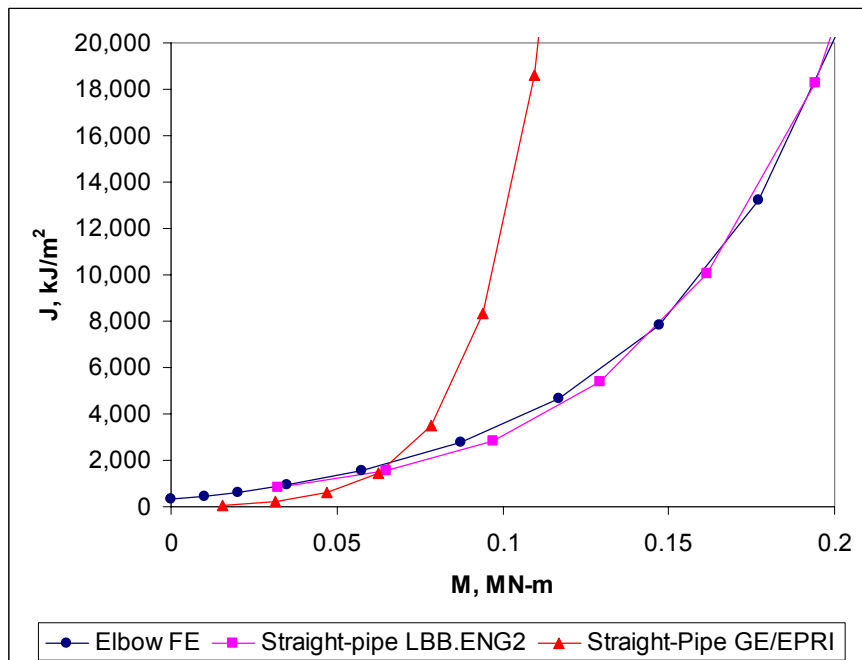


Figure F.19 Comparison of J versus moment curves for a circumferential through-wall crack in a straight pipe and centered on the extrados of an elbow with an $R/t = 20$ and $2\theta = 180$ degrees

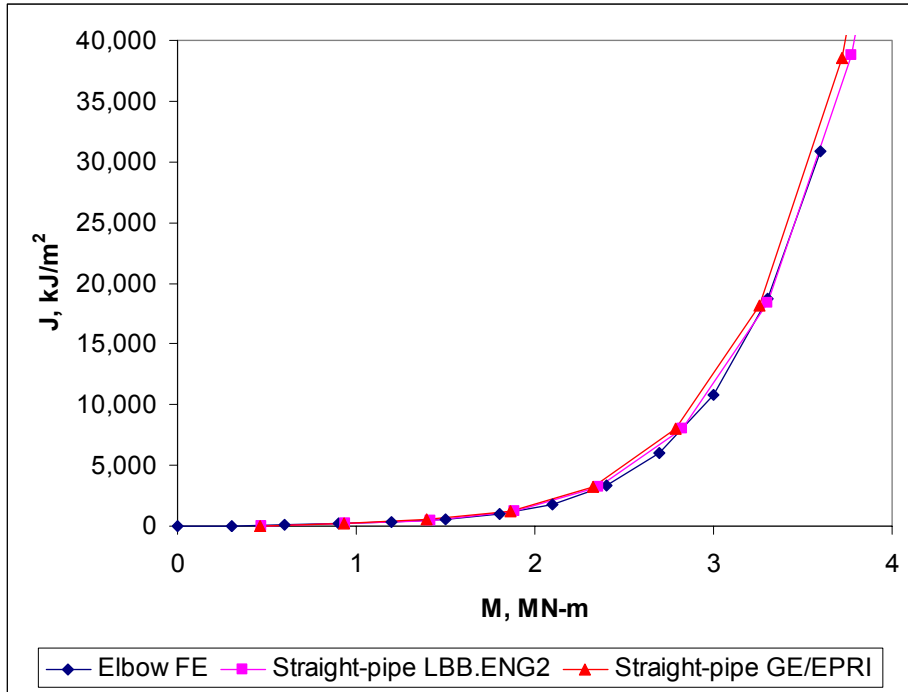


Figure F.20 Comparison of J versus moment curves for a circumferential through-wall crack in a straight pipe and centered on the extrados of an elbow with an $R/t = 5$ and $2\theta=90$ degrees

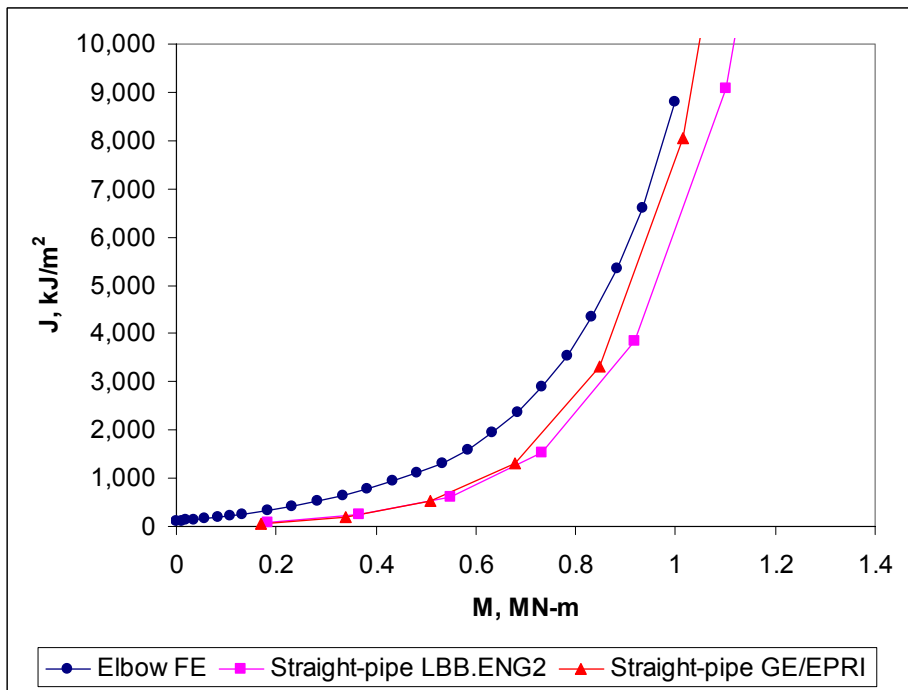


Figure F.21 Comparison of J versus moment curves for a circumferential through-wall crack in a straight pipe and centered on the extrados of an elbow with an $R/t = 5$ and $2\theta=180$ degrees

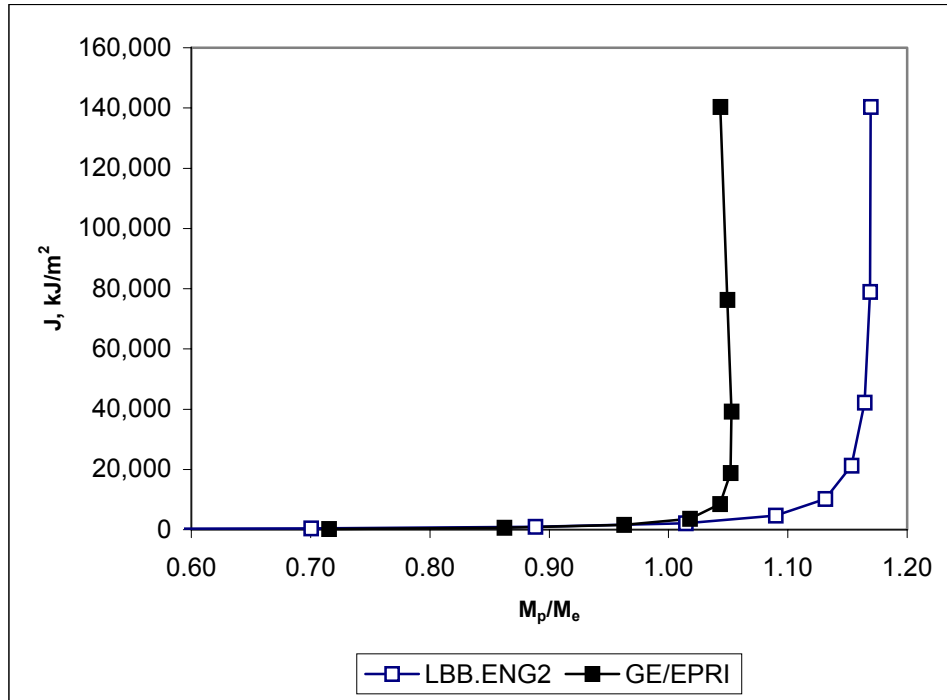


Figure F.22 Comparison of J versus moment ratios for a circumferential through-wall crack in a straight pipe and centered on the extrados of an elbow with an $R/t = 20$ and $2\theta=90$ degrees

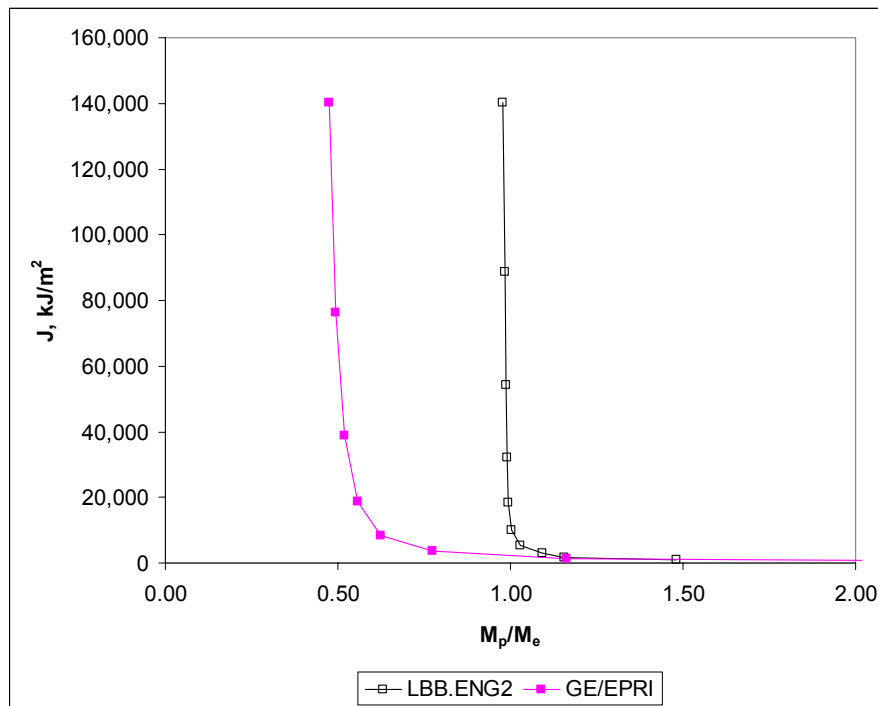


Figure F.23 Comparison of J versus moment ratios for a circumferential through-wall crack in a straight pipe and centered on the extrados of an elbow with an $R/t = 20$ and $2\theta=180$ degrees

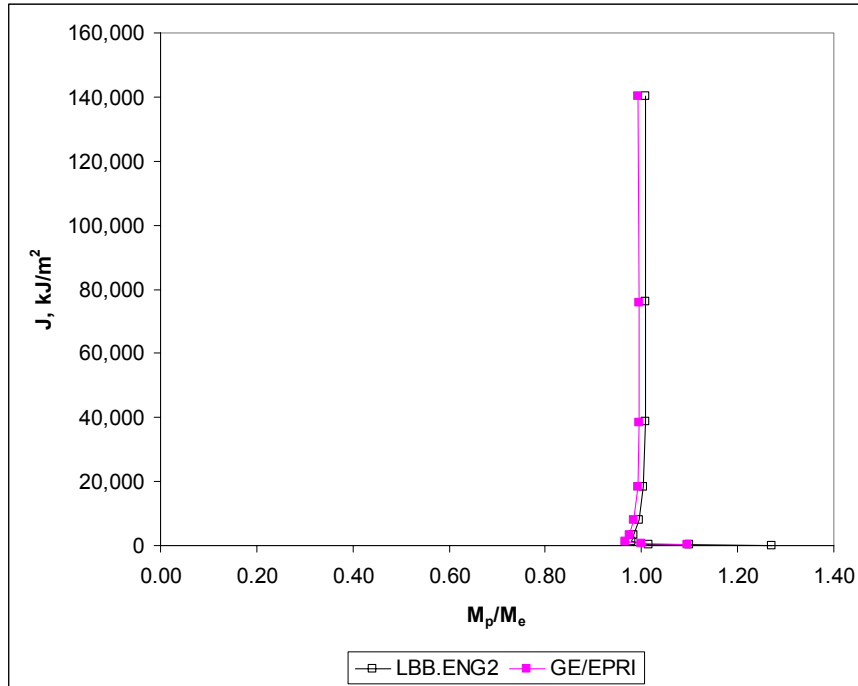


Figure F.24 Comparison of J versus moment ratios for a circumferential through-wall crack in a straight pipe and centered on the extrados of an elbow with an $R/t = 5$ and $2\theta=90$ degrees

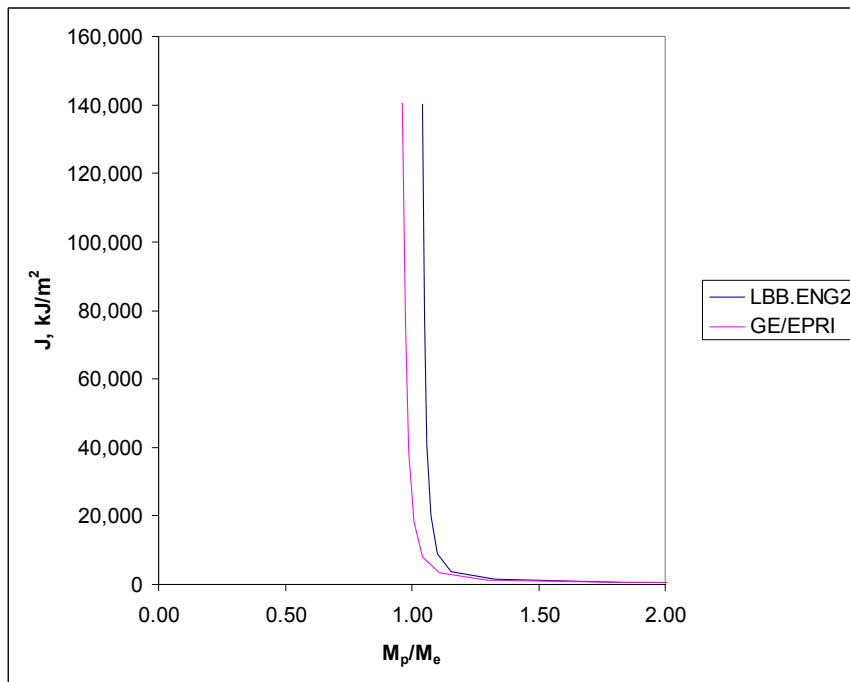


Figure F.25 Comparison of J versus moment ratios for a circumferential through-wall crack in a straight pipe and centered on the extrados of an elbow with an $R/t = 5$ and $2\theta=180$ degrees

The final step was to compare the constant moment ratio values from Figures F.22 to F.25 to the stress indices for the elbows. Since the elbow was under bending, the ASME B_2 index was used. The B_2 index is for primary bending stresses to avoid failure by collapse (using the design stress analysis definition of limit load). It should be noted that the elbow stress indices essentially gives a stress multiplier for the location in the piping product where the stresses are the highest. For the case of an elbow under bending, the stresses are the highest along the flank of the elbow normal to the axial direction. Equations F.25 and F.26 define the B_2 stress index from Section III, Article NB-3683.7 of the ASME Boiler and Pressure Vessel Code.

$$B_2 = 1.3h^{2/3}, B_2 \geq 1.0 \quad (\text{F.25})$$

Where,

$$h = tR_{el} / R_m^2 \quad (\text{F.26})$$

These equations assume the elbows have a perfectly circular cross section, which was a

condition in the development of the FE elbow results.

The results of this comparison are shown in Figure F.26. If there is essentially no effect of the elbow curvature on the fracture behavior, then the moment ratios should be close to 1.0 for all B_2 values. On the other hand, if there was a strong effect of the elbow curvature, then the moment ratios should be close to the 45-degree line in Figure F.26. As can be seen in Figure F.26, the values are all close to 1.0 indicating that for a circumferential through-wall flow in an elbow that the straight-pipe solution could be used.

There was one data point that gave an $M_{\text{pipe}}/M_{\text{elbow}}$ value of about 0.5. This was when the GE/EPRI solution was used for the case of a 180-degree flaw in pipe with an R/t of 20. However, we know that the solution in this case is not correct in NRCPIPE so that this data point can be disregarded. Consequently, the circumferential through-wall-flaw straight-pipe solution could be used in the new LBB Regulatory Guide for the fracture analyses of the case of a circumferential through-wall flaw in an elbow.

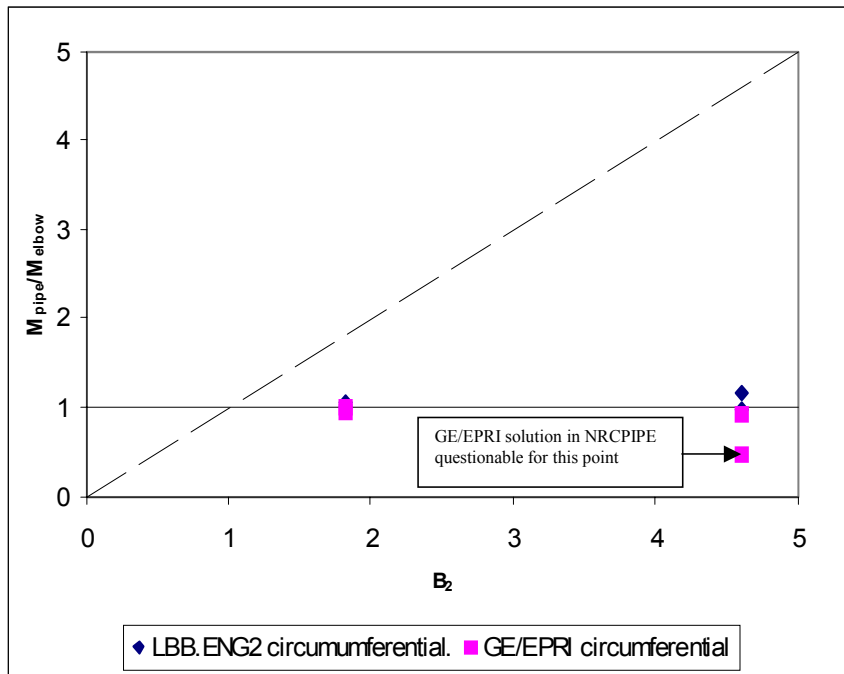


Figure F.26 Ratio of circumferentially through-wall-cracked pipe-to-elbow moments for constant applied J values versus the ASME B_2 index for the elbow

F.8.2.3 Comparison of Axial Flank Through-Wall-Cracked Elbow and Straight-Pipe

Solutions - To make this comparison, the J versus moment curves from both the straight-pipe and elbow solutions were compared in a similar manner as was done for the elbow circumferential crack case. Figures F.27 and F.28 show the results for the axial flank crack case with an R/t of 20 and total crack lengths of 15 and 30 degrees. Figures F.29 and F.30 show the results for the axial flank crack case with an R/t of 5 and total crack lengths (2) of 15 and 30 degrees.

In Figures F.27 to F.30, it can be seen that the elbow solutions give higher J values than the straight pipe solutions for the same moment. The GE/EPRI solution always gives a higher crack-driving force than the LBB.ENG2 analysis for the two straight-pipe solutions. This is consistent with past experience. The crack lengths are much shorter in these analyses than what was used in the circumferential cracked elbow analysis, so that there was no problem with either straight-pipe solution in the NRCPIPE code.

The next step was to compare the ratio of the moments at the same J value. A graph of the moment ratio versus the J value is given for each case in Figures F.31 to F.34. Again note how the moment ratio reaches a constant value as the plastic solution of J dominates.

The final step was to compare the constant moment ratio values from Figures F.31 to F.34 to the B_2 stress indices for the elbows.

The results of this comparison are shown in Figure F.35. If there is essentially no effect of the elbow curvature on the fracture behavior, then the moment ratios should be close to 1.0 for all B_2 values. On the other hand, if there was a strong effect of the elbow curvature, then the moment ratios should be close to the 45-degree line in Figure F.35.

As can be seen in Figure F.35, the moment ratio values show that there is an effect of the elbow curvature on the crack-driving force for an axial through-wall crack on the flank of an elbow. A conservative option would be to divide the circumferential through-wall straight-pipe moment by the elbow B_2 value for an axial through-wall flaw on the flank of the elbow. Alternatively, a linear correction such as suggested by the lines in Figure F.35 could be used. Consequently, the moment from a circumferential through-wall-flaw straight-pipe solution (under pressure and bending) divided by the elbow B_2 stress index could be used in the new LBB Regulatory Guide for the fracture analyses for the axial flank through-wall flaw case in an elbow.

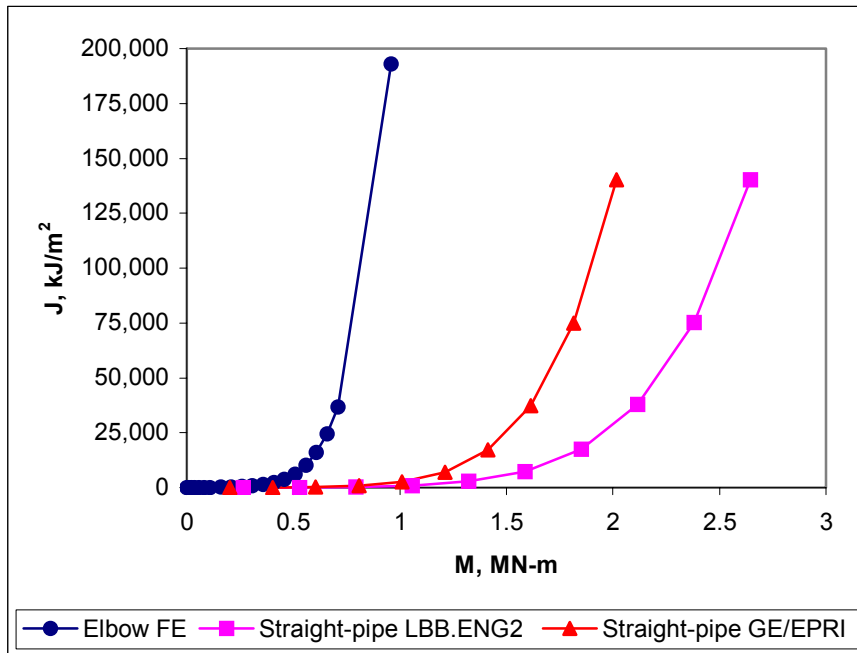


Figure F.27 Comparison of J versus moment curves for an axial through-wall crack in a straight pipe and an axial through-wall crack on the flank of an elbow with an $R/t = 20$ and $2\theta=15$ degrees

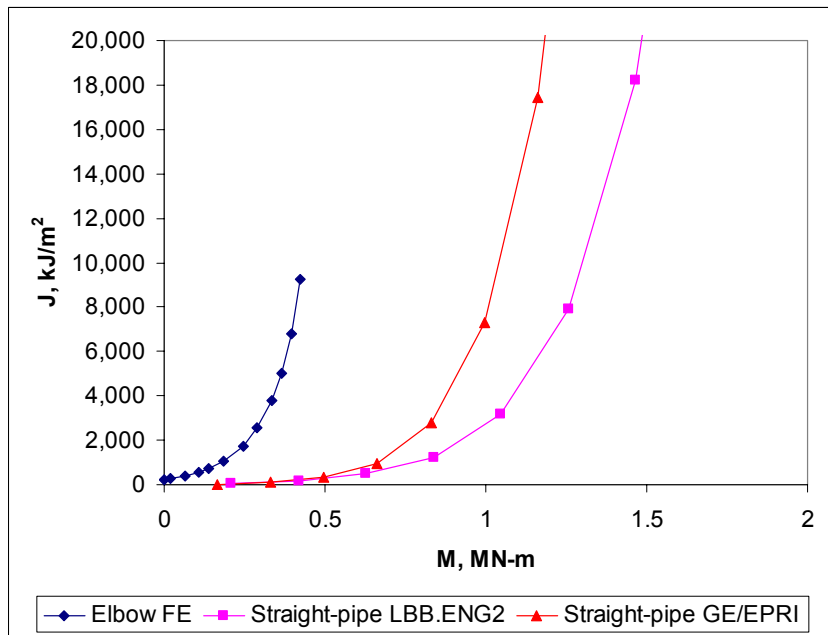


Figure F.28 Comparison of J versus moment curves for an axial through-wall crack in a straight pipe and an axial through-wall crack on the flank of an elbow with an $R/t = 20$ and $2\theta=30$ degrees

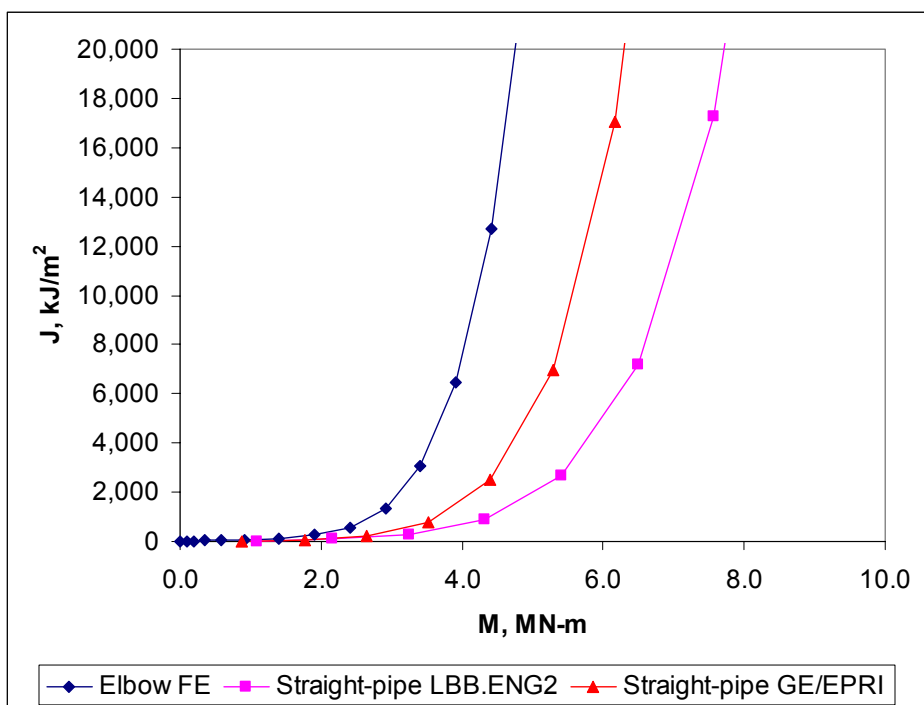


Figure F.29 Comparison of J versus moment curves for an axial through-wall crack in a straight pipe and an axial through-wall crack on the flank of an elbow with an $R/t = 5$ and $2\theta = 15$ degrees

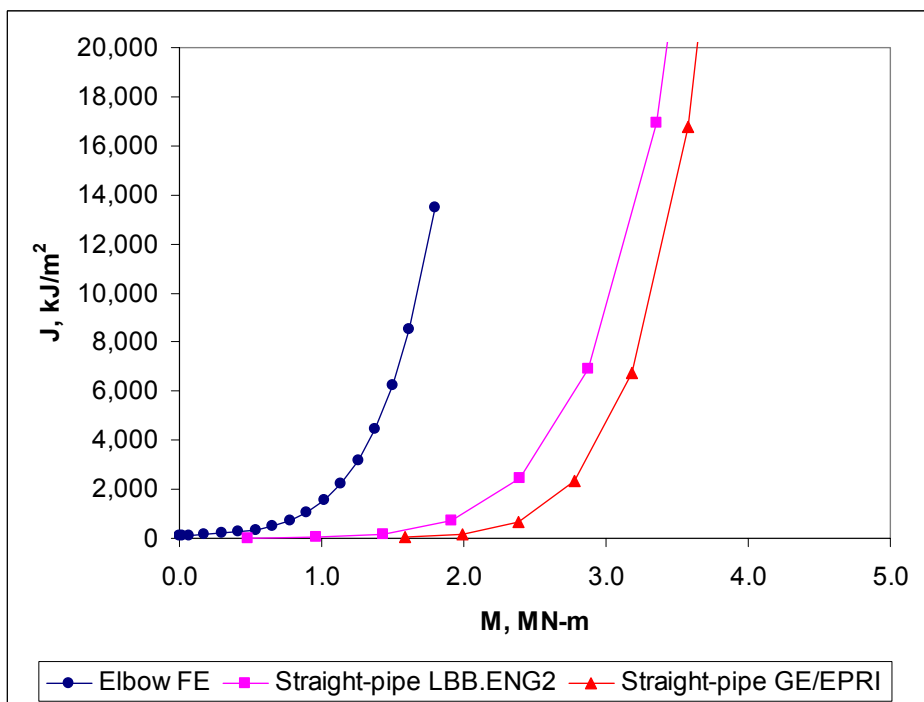


Figure F.30 Comparison of J versus moment curves for an axial through-wall crack in a straight pipe and an axial through-wall crack on the flank of an elbow with an $R/t = 5$ and $2\theta = 30$ degrees

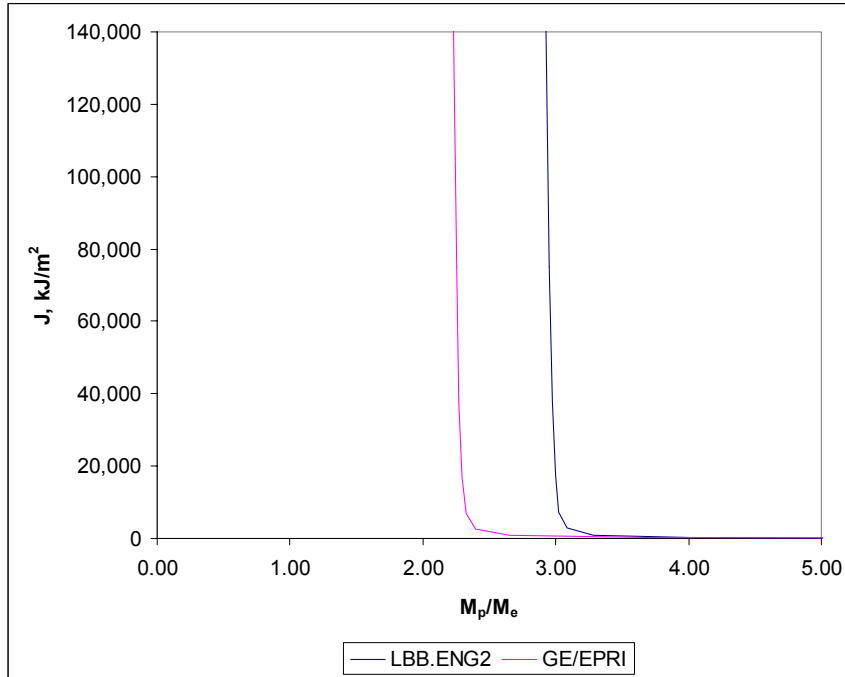


Figure F.31 Comparison of J versus moment ratios for an axial through-wall crack in a straight pipe and an axial through-wall crack on the flank of an elbow with an $R/t = 20$ and $2\theta=15$ degrees

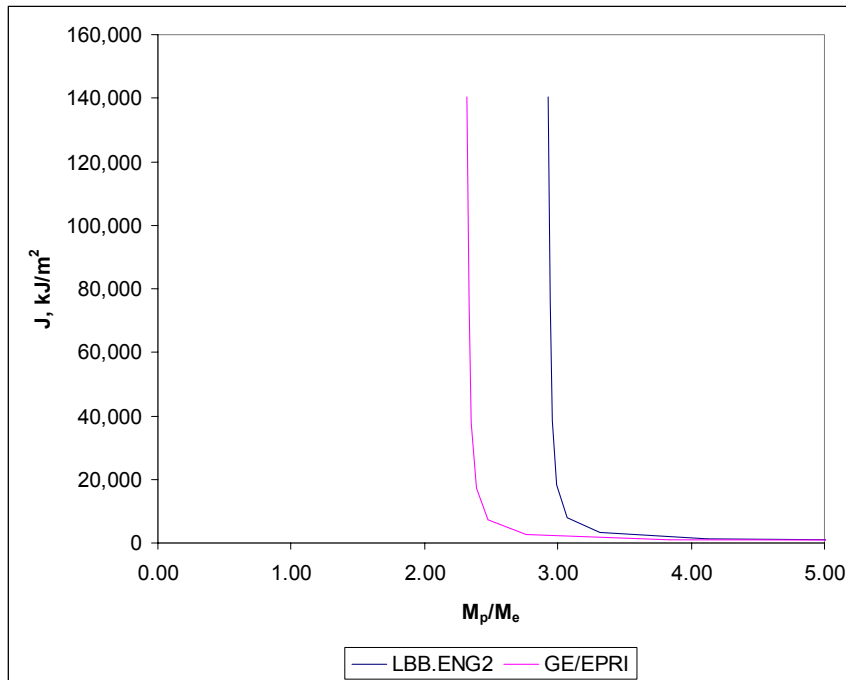


Figure F.32 Comparison of J versus moment ratios for an axial through-wall crack in a straight pipe and an axial through-wall crack on the flank of an elbow with an $R/t = 20$ and $2\theta=30$ degrees

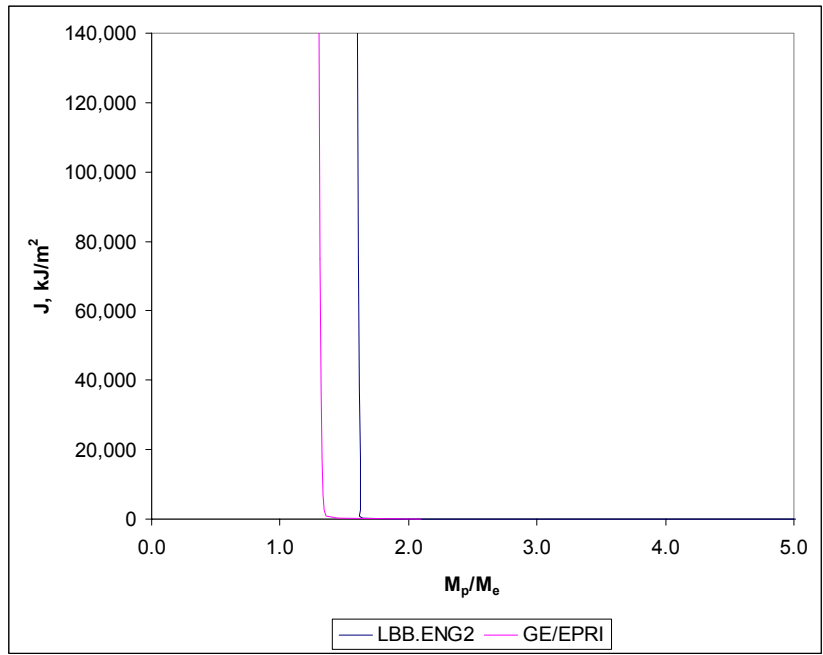


Figure F.33 Comparison of J versus moment ratios for an axial through-wall crack in a straight pipe and an axial through-wall crack on the flank of an elbow with an $R/t = 5$ and $2\theta=15$ degrees

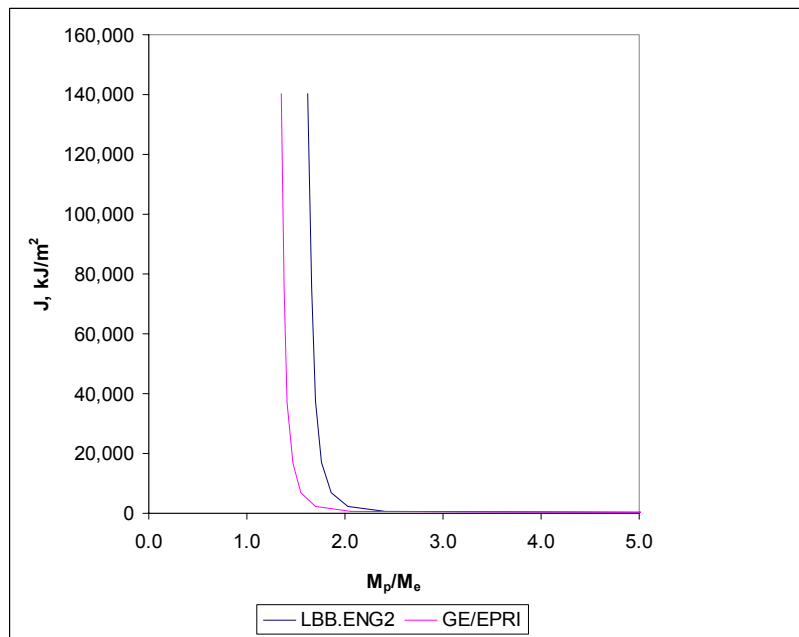


Figure F.34 Comparison of J versus moment ratios for an axial through-wall crack in a straight pipe and an axial through-wall crack on the flank of an elbow with an $R/t = 5$ and $2\theta=30$ degrees

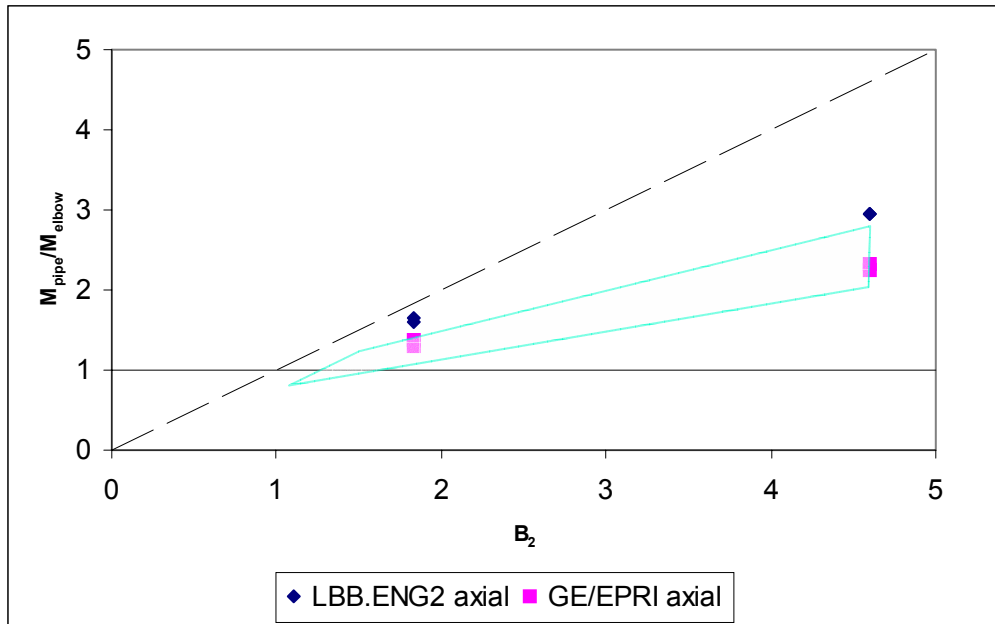


Figure F.35 Ratio of axially through-wall-cracked pipe-to-elbow moments for constant applied J values versus the ASME B₂ index for the elbow

F.8.2.4 Comments on Crack-Opening

Displacement - The analyses conducted in Sections F.8.2.2 and F.8.2.3 for circumferential and axial through-wall cracks in elbows, respectively, were for determining the crack-driving force when plasticity occurs. This would be valid for the LBB fracture assessment under normal plus SSE loads. The crack-opening displacement, however, occurs under more elastic loading conditions. It was beyond the scope of this effort to make those comparisons, and using the same B₂ correction approach should be used with caution with the COD analysis.

F.8.3 Summary and Conclusions

The objective of this evaluation was to determine if a more simplified analysis could be established for axial and circumferential through-wall cracks in elbows under combined pressure and bending. This was assessed by using the elbow finite element analyses developed as part of this effort with a hoop stress loading of 1.0 S_m for typical nuclear piping steels. The approach undertaken was to compare the ratio of the moments for the same size crack in an elbow and straight-pipe at the

same applied J values. This was similar to efforts done for circumferential surface flaws in elbows in the IPIRG-2 program. The following conclusions came from this analysis.

- The results of the analysis showed that a circumferential crack centered on the extrados of an elbow had the same crack-driving force under plastic conditions as a circumferential through-wall crack in a straight pipe. Hence, for the new LBB Reg. Guide, the simple straight-pipe solutions could be used for the fracture analysis of a circumferential through-wall crack in an elbow.
- The results of the analysis showed that an axial crack on the flank of an elbow had a higher crack-driving force under plastic conditions than a circumferential through-wall crack in a straight pipe. A conservative approach would be to use the straight-pipe solution, but divide the straight-pipe moment by the elbow B₂ index. This could readily be done in the new LBB Reg. Guide Level 1 or 2 analyses for the fracture analysis of an axial flank through-wall crack in an elbow.

- The COD evaluations were not conducted in this effort. Caution should be used in applying this same approach for the COD values since the COD should be for elastic loading where the constant moment ratio that occurs under plastic conditions does not exist.

F.9 References

F.1 Mohan, R., Brust, F. W., Ghadiali, N. D., and Wilkowski, G. M., "Development of a J-Estimation Scheme for Internal Circumferential and Axial Surface Cracks in Elbows", NUREG/CR 6445, June, 1996.

F.2 Kumar, V., German, M., and Shih, E., "An Engineering Approach for Elastic-Plastic Fracture Analysis ", EPRI Report No. NP-1931, July 1981.

F.3 Kumar, V., German, M., Wilkening, Andrews, W., deLorenzi, H., and Mowbray, D., "Advances in Elastic-Plastic Analysis " EPRI Final Report NP-3607, August 1984.

F.4 Kumar, V., and German, M. D., "Elastic-Plastic Fracture Analysis of Through-Wall and Surface Flaws in Cylinders", EPRI Final Report NP-5596, January, 1988.

F.5 P. Gilles and F. W. Brust, "Approximate Fracture Methods for Pipes, Part I, Theory", Nuclear Engineering and Design, Vol. 127, pp. 1-17, 1991.

F.6 P. Gilles, K. S. Chao, and F. W. Brust, "Approximate Fracture Methods for Pipes, Part II, Applications," Nuclear Engineering and Design , Vol. 127, pp. 19-31, 1991.

F.7 Scott, P. M., and Ahmad, J., "Experimental and Analytical Assessment of Bending Circumferentially Surface-Cracked Pipes Under Bending", NUREG/CR-4872, April 1987.

F.8 Rahman, S. and Brust, F. W., "Approximate Methods for Predicting J-integral of a Circumferentially Surface-Cracked Pipe Subject

to Bending," International Journal of Fracture, Vol. 85, No. 2, October 1997, pp. 111-130.

F.9 Brust, F., Scott, P., Rahman, S., Ghadiali, N., Kilinski, T., Francini. R., Krishnaswamy, P., and Wilkowski, G., "Assessment of Short Through-Wall Cracks in Pipes - Experiments and Analyses," Topical Report, NUREG/CR-6235, U. S. Nuclear Regulatory Commission, Washington, DC, April 1995

F.10 Krishnaswamy, P., Scott, P., Choi, Y., Mohan, R., Rahman, S., Brust, F., and Wilkowski, G., "Fracture Behavior of Short Circumferentially Surface-Cracked Pipe," Topical Report, NUREG/CR-6298, U. S. Nuclear Regulatory Commission, Washington, DC, November 1995.

F.11 Rahman, S., and Brust, F. W., "Elastic-Plastic Fracture of Circumferential Through-Wall Cracked Pipe Welds Subject to Bending", ASME Journal of Pressure Vessel Technology, Vol. 114, pp 410-416, November, 1992.

F.12 Mohan, R., Krishna, A., Brust, F. W., and Wilkowski, G., " J-estimation Scheme for Internal Circumferential and Axial Surface Cracks in Pipe Elbows," ASME J. of Pressure Vessel Technology, Vol. 120, Nov. 1998.

F.13 Kilinski, T., and others, "Fracture Behavior of Circumferentially Surface-Cracked Elbows," NUREG/CR-6444, December 1996.